PRESSURE DISTRIBUTION
ON A ROTATING
AXIAL-FLOW COMPRESSOR BLADE

by

Per Erik Schultz

Thesis submitted to the Graduate Faculty of the
Virginia Polytechnic Institute and State University
in partial fulfillment of the requirements for the degree of

MASTER OF SCIENCE

in

Mechanical Engineering

APPROVED:

H. L. Moses

W. F. O'Brien, Jr

E. F. Brown

August, 1976

Blacksburg, Virginia

II. ACKNOWLEDGEMENTS

The author expresses sincere appreciation to members of his advisory committee: Professors E. F. Brown, W. F. O'Brien, Jr., and H. L. Moses, Chairman. The latter two professors were especially helpful throughout the investigation. The author is very obliged to

for permission to use the finite-difference blade-to-blade computer program.

III. TABLE OF CONTENTS

TABLE OF CONTENTS (Continued)

IV. LIST OF FIGURES

IV. LIST OF FIGURES (Continued)

V. LIST OF TABLES

VI. LIST OF SYMBOLS

B.L.	boundary layer
C	absolute velocity
C_f	skin friction coefficient
e	internal energy per unit mass
f	body forces
g	gravitational forces
k	thermal conductivity
P	static pressure
P_o	total pressure
r	radius
Re	Reynolds number
t	time
U	blade velocity
U_e	free stream velocity
$\bar{u}$	average velocity in boundary layer
u	velocity in x-direction
u_i, u_j, u_k	velocities in tensor form
v	velocity in y-direction
α	angle to absolute velocity
β	angle to relative velocity
δ	boundary layer thickness
γ	stagger angle
λ	second viscosity coefficient

μ	dynamic viscosity
ν	kinematic viscosity
ρ	density
ψ	stream function
ω	vorticity

Subscripts

a	axial
c	centrifugal
r	relative to the blade
w	whirl
i,j,k	tensor notation
1	upstream of rotor
2	downstream of rotor

VII. INTRODUCTION

Higher efficiency and lighter units are desired goals in the efforts to obtain better compressors and turbines. These goals are not achieved by merely knowing the inlet and outlet conditions for the flow in stationary compressor blades. It is, however, easy to obtain experimental data for these conditions, so there are many methods to deduce the compressor performance from this approach. Nevertheless, a better understanding of the flow behavior around the blades, and especially in the area close to the surface, is of great importance. Much research has been and is being done to determine the nature of the flow in compressors, particularly in the stall region and pre-stall region.

The general equations governing the flow around the blades are very complex. It is a very cumbersome, if not impossible, procedure to obtain an analytical solution for the flow field unless a high degree of simplification is made. To be able to justify the simplifications made, it is of great importance to have access to reliable experimental results for comparison.

The complexity of the flow is due to a large variety of factors such as; the flow is compressible, three dimensional, turbulent and viscous and in addition, the flow is known to be unsteady and perhaps separated. In some cases the flow is partly supersonic and partly subsonic, and thus effected by local shock waves.

In the development of an analytical solution, the area of investigation usually is considered to be the flow field between a pair of

adjacent compressor blades. The assumptions often made for the flow are; the flow is considered to be in steady motion, the flow is regarded as that of an ideal non-viscous fluid, and the fluid is incompressible. These assumptions are made everywhere in the flow field except close to the blade surface, where boundary layer theory is used. To solve for the flow mathematically it is usually assumed to be irrotational. The condition of irrotationality allows the introduction of a potential function from which the velocities can be determined. The theoretical performance for the compressor may be deduced from these velocities. Comparison of the theoretical performance with experimentally obtained results enables conclusions of the applicability of the theory used, and the justification for employing certain assumptions is sometimes questioned.

The purpose of this investigation is to achieve accurate experimental data for the pressure distribution on a rotating axial-flow compressor blade. The experimental results are compared with theoretically obtained solutions. The investigation includes the region from design conditions through stall conditions for the compressor. For the experiments special blades have been made for measuring the pressure on the blade surface. A scanning valve has been purchased which selects from where the pressure information is to be taken. This valve transmits the pressure signal to one very stable stationary transducer, from which an analog electrical signal is obtained. This signal, due to a low pass filter, corresponds to the mean pressure. Elimination of centrifugal effects on blade-mounded pressure transducers is gained by this procedure.

VIII. REVIEW OF LITERATURE

Through the years there have been many investigations in the compressor flow area. The earliest of these have mainly investigated the flow in stationary cascades of blades, both cylindrical and straight. This is due to the difficulties connected with on-rotor measurements. Some compared the experimentally obtained data with analytical solutions for the flow field. Because of the complexity of the problems involved with compressor flow theory, the analyses had to be simplified. Modern computers have made it possible to obtain fast and accurate analytical solutions for the flow field. However, the equations governing the flow field still have to be simplified.

Historical Review

In 1947 Weske [1] investigated the aerodynamic characteristics of a rotating axial-flow blade grid with pressure increasing effects. He provided one of his blades, which he referred to as the master blade, with several pressure taps arranged in three different span positions (87.5%, 50%, and 12.5% span). The outer and the inner position was one inch from the housing and hub respectively, to avoid the end-wall boundary layers. Each span position had 23 taps, and these were distributed equally over the pressure and suction sides. From these taps he obtained the pressure distribution over the blade surface. The purpose of the investigation was to analyze the flow through the rotating grid. The emphasis was on those effects not existing in a non-rotating grid and on the factors not included in the

two-dimensional theory for axial flow blade grids. Certain effects, such as centrifugal acceleration, was impossible to simulate in a stationary test. Weske found that the tip section stalled early and the root section late due to radial displacement of the boundary layer. He also found that this effect could precipitate "pumping" as a result of tip stall and certainly decrease the efficiency.

The same year Weske also published [2] an additional article on certain aspects of flow in compressors and turbines. Here he investigated flow in boundary layers and wakes encountered in multiple blade rows qualitatively, especially in connection with operating characteristics. He investigated the use of two-dimensional theory to incorporate corrections for the three-dimensional effects. Weske determined that on single stage units the boundary-layers were relatively thin so that the three-dimensional effects were relatively small and probably negligible, whereas on multistage units these three-dimensional effects were of importance. A criterion for radial stability was proposed and defined. This criterion used the relation between the radial distribution of pressure versus the magnitude of the radial distribution of the whirl velocity.

In an investigation also made in 1947, Runckel and Davey [3] explored the pressure distribution about the mean span on the rotating blades of a single-stage axial-flow compressor. The pressure transfer device they used contained mercury to obtain the seal necessary between rotating and stationary parts. The apparatus they employed had 24 cells, which allowed them to transmit 24 pressures coincidentally. Their

conclusions were that the maximum suction side pressure, for the thin low chambered blade they used, was hardly greater than for the isolated airfoil of the same section. Furthermore, they determined the necessity of using cascade test data to design the blade angles for the rotor, since the experimental lift curve slope was much lower than that estimated from theoretical calculations. The compressor employed was found to stall first at the root and tip sections of the blades due to casing boundary-layer effects, incorrect blade twist and large clearances.

At Lewis Flight Propulsion Laboratory in Cleveland, Ohio, Wu and Wolfenstein [4] in 1949 analyzed the radial motion and radial equilibrium condition in an axial-flow compressor. They concluded that even in free-vortex designs, with non-tapered passage walls and requiring no change in velocity distribution from stage to stage, a conceivable amount of "oscillatory radial motion" takes place within the stage. These effects are of such a significant magnitude that they should be regarded in the design. The determination of the "oscillatory radial motion" required a long process of step-by-step calculations. It was found, however, that a sinusoidal radial flow path gives good approximate results. The method usually employed for calculations and hence design, neglecting the radial motion, is correct enough only for the case in which the axial length of the blade row is much longer than the radial length, and is incorrect for use in the case of a finite blade-row aspect ratio. The differences between the method Wu and Wolfenstein suggest and the usual method

are significant.

In 1951 Westphal and Godwin [5] utilized the pressure transfer device that Runckel and Davey [3] had developed. They compared the performance of a NACA-65 compressor blade in a two-dimensional cascade with the performance of the same blade in an axial-flow compressor with a rotor of free-vortex type. They measured inlet and exit velocities, pressure rise, and the pressure distribution on the blade surface. While Runckel and Davey [3] only measured midspan, Westphal and Godwin employed three different span locations in a manner similar to that of Weske [1]. The comparison indicated that the data obtained from the cascade quite accurately predicts turning angles and blade pressure distributions on the compressor, but only for the compressor design angle of attack. At other than design angle of attack, the comparison showed significant differences, probably due to secondary flows.

Schlichting [6] did in 1954 a comprehensive investigation on both a straight and a cylindrical cascade. He compared the experimental results with analytical results. Schlichting obtained for the first time theoretical data on the loss coefficient by applying boundary-layer theory. Due to the lack of computers, an extensive computation of "cascade down-wash tables" was necessary to decrease the amount of work to such an extent that it was possible to obtain a systematic theoretical investigation of the cascade. He noticed in a comparison of tests on two-dimensional cascades with tests on cylindrical cascades that the effects of radial divergence on the pressure distri-

bution on a blade and on the local loss coefficient were insignificantly small. Schlichting approached the cascade flow problem in two ways, the "indirect problem" approach and the "direct problem" approach. In the indirect problem the known quantities were the velocity diagram (velocity triangles) for the inlet and exit and the geometry of the cascade was unknown. In the direct problem the known quantities were the geometry of the cascade and the geometry of the blade profile. In both the direct and indirect problem, the pressure distribution on the blade surface was an unknown quantity. As a result of this investigation, Schlichting obtained a solution for the two-dimensional frictionless cascade for both the direct and the indirect problem. He used the Prandtl-Glauert rule to relate incompressible flow to compressible subsonic flow.

In 1956 Johnson and Bullock [7] issued a comprehensive work on the "aerodynamic design of axial-flow compressors." First the work was regarded as confidential, but after 1958 the general public had access to it. This work was an attempt to take in all earlier research in the axial-flow compressor area and to correlate this information into a single report, which hopefully should be of value in compressor design.

At Virginia Polytechnic Institute and State University, there is a continuing investigation in the axial-flow compressor field (References 9, 10 and 11). The work reported here is a part of that effort.

IX. THE INVESTIGATION

The objective of the experiments was to obtain accurate experimental mean pressure data on the rotating axial-flow compressor blade. The pressure data was obtained from three different span positions. Radial equilibrium was used to calculate the velocities at radii different from mean radius data.

The intention of the analytical investigation was to accomplish a potential flow solution for the velocity distribution on the blade surface. The boundary-layer displacement thickness was added to the blade to simulate viscous flow.

The experimental equipment, procedures, data acquisition and data evaluation are described in Part 1.

The procedures and analysis from the analytical approach are described in Part 2.

Part 1

A. Experimental Equipment

Axial-Flow Compressor

The compressor employed in this investigation was manufactured by General Electric and has the model number 5GDY34A1. The unit consists of an axial-flow fan direct coupled to and mounted on a common non-self-supporting bedplate with a 5.5 kW DC cradled dynamometer. It is possible to operate the compressor as a single-stage or as a two-stage machine. Throughout these experiments, only the

single stage configuration was used.

As employed in this investigation, the compressor unit consists of one stator section, acting as inlet guide vanes, and one rotor section. The compressor is shown in Figure 1.

The stator contains 37 adjustable inlet guide vanes attached to the outer casing upstream of the rotor. The stator was set at an angle of 16 degrees at the mean radius for the experiments. The blade angle setting is shown in Figure 2. The stator angles have a twist of 8 degrees, and thus the root angle was 12 degrees and the tip angle was 20 degrees. The vanes were arranged to supply a whirl velocity in the opposite direction from the rotor motion (Figure 10).

The rotor has 24 adjustable blades with a blade twist of 4 degrees. The rotor blades have a RAF #6 cross section (Figure 3). The rotor blades have a chord length of 42.3 mm and a span length of 70.2 mm. The rotor hub diameter is 310.6 mm, thus making the blade root to tip ratio 0.687. The outer casing diameter is 451.8 mm with a nominal tip clearance of 0.38 mm. The rotor blades have a solidity ratio of 1.18 at mean radius. For the experiments, a mid-span blade angle of 60 degrees was utilized, which makes the angle at the hub 58 degrees and the angle at the tip 62 degrees. Figure 2 shows the angle setting at mid-span. The rotor is seen in the photograph of Figure 4.

The fan is arranged to discharge into a 122x122x122 cm plenum (Figure 5). A discharge valve connecting the output from the plenum to a 45.7 cm duct controls the compressor mass flow rate. Table 1 shows the angle of attack versus the valve positions used. The angle

FIGURE 1. PHOTOGRAPH OF THE COMPRESSOR AND GENERAL TEST SET UP

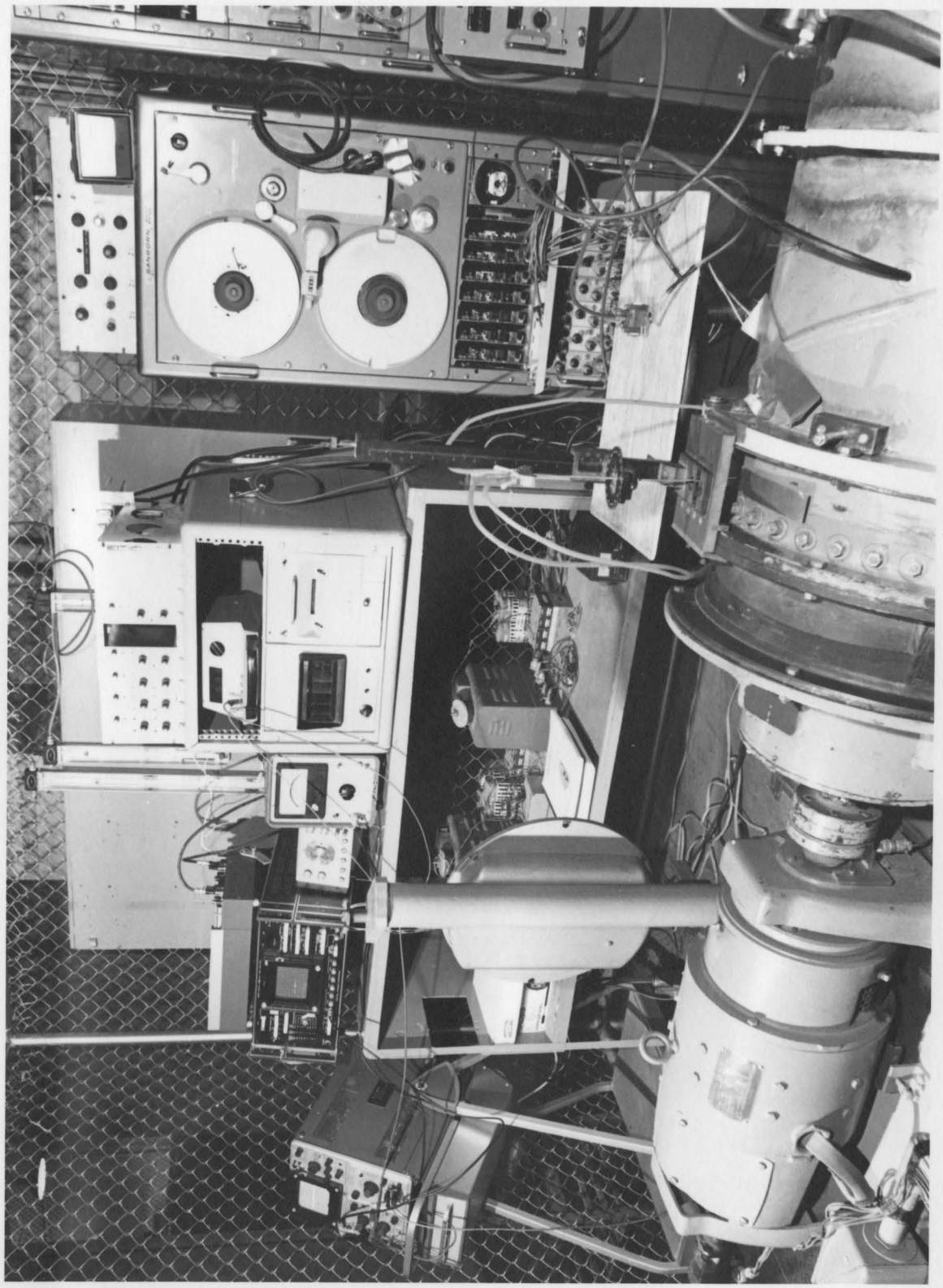

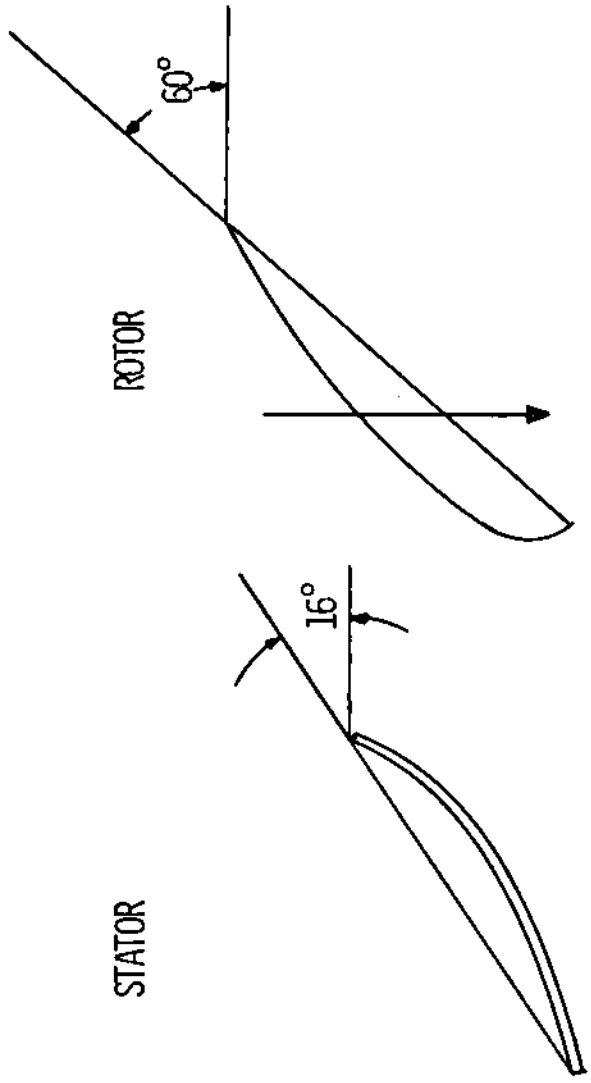

FIGURE 2. STATOR AND ROTOR BLADE ANGLE SETTINGS

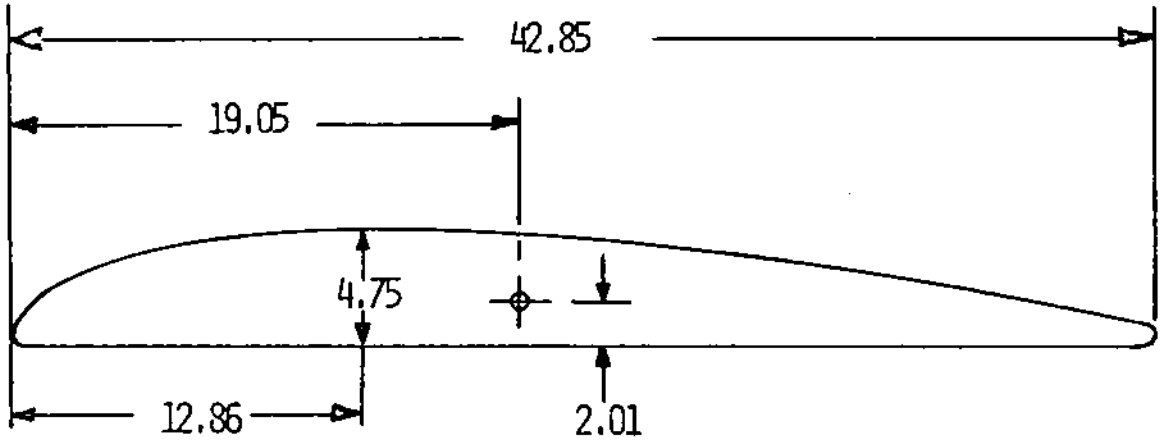

FIGURE 3. CROSS SECTION OF RAF #6 PROPELLER SECTION

FIGURE 4. PHOTOGRAPH OF THE SCANIVALVE AND THE ROTOR

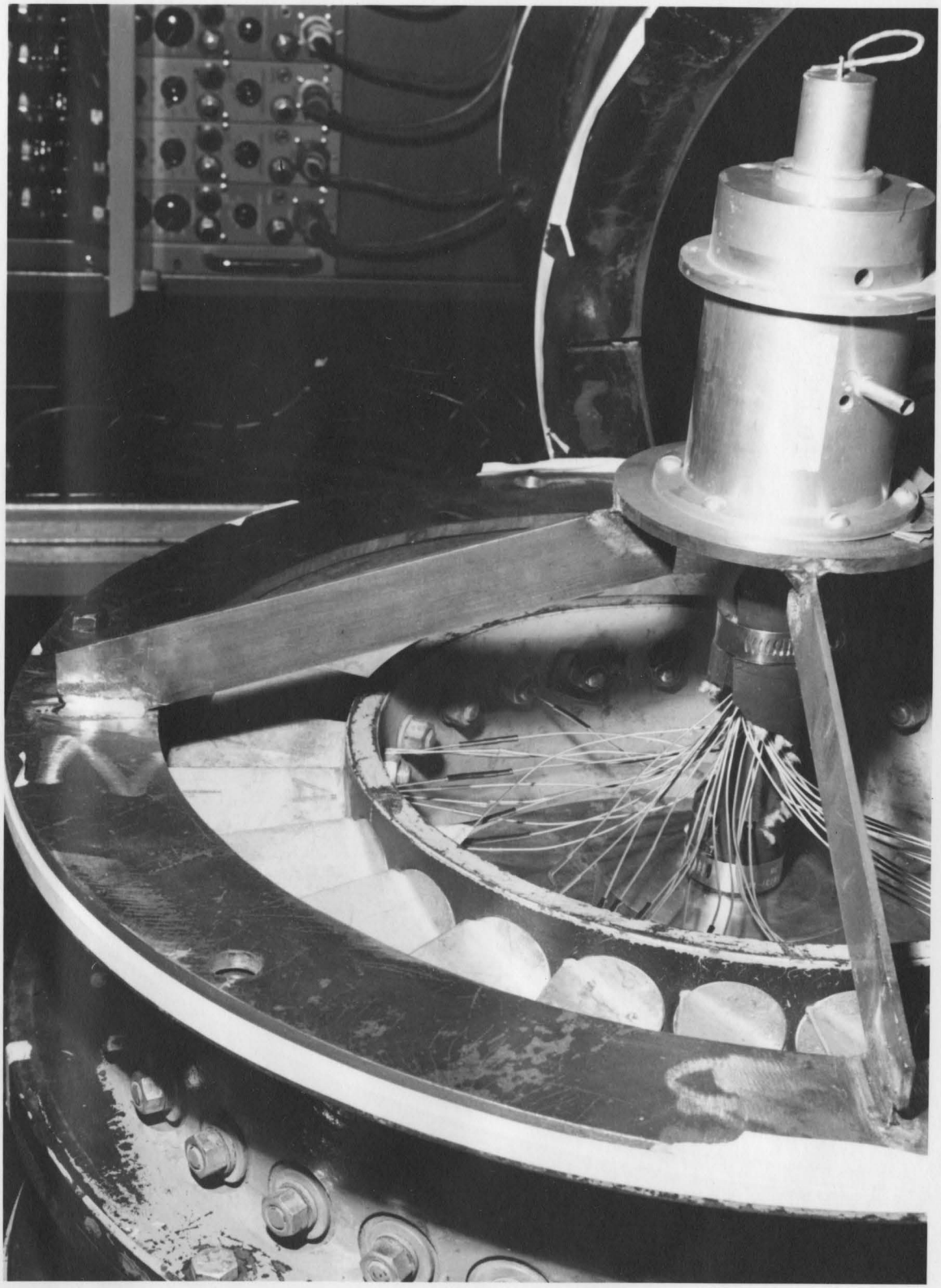

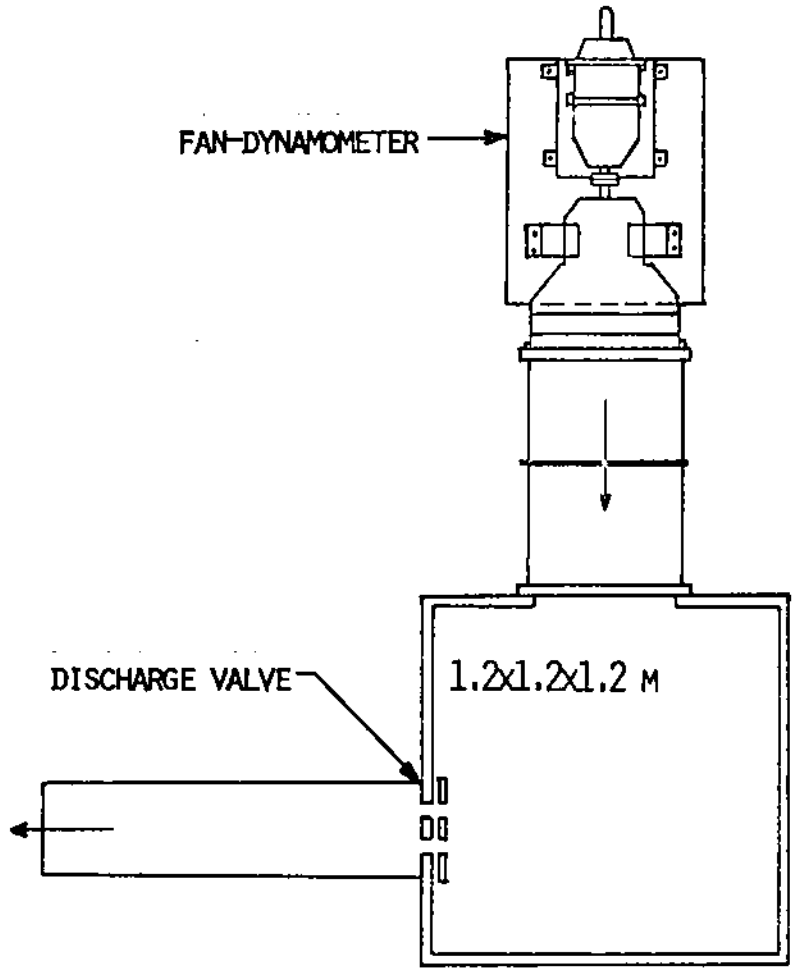

FIGURE 5. COMPRESSOR, PLENUM AND EXHAUST DUCTING ARRANGEMENTS

Table 1. Valve Position Versus
Angle of Attack

valve position	angle of attack
0	4.4°
1	5.3°
2	5.7°
3	6.2°
4	7.2°
5	8.9°
6	10.7°
7	11.9°
8	(13.4°)
9	(12.8°)

Note: Due to large fluctuations associated with stall at large angles of attack (valve position 8 and 9) the data is not completely reliable in this region.

of attack is calculated as shown in Part C.

The compressor is driven by a 5.5 kW variable speed, cradled dynamometer. The dynamometer speed can be varied over a range of 500 RPM to 3000 RPM. The minimum speed is limited because of inadequate ventilation and cooling at lower speeds. The only speed used in the experiments was 2400 RPM. The dynamometer scale and tachometer permitted measurement of power supplied to the compressor.

Pressure Scanner

The pressure scanner employed, henceforth referred to as the Scanivalve,[R] was manufactured by the Scanivalve Corporation and had the model number 36 TR. The Scanivalve has 36 ports for pressure measurement, however, in the experiments only 31 were adapted. The Scanivalve scanned the ports one at a time with a manually controlled speed. The stepping was achieved by an air-stepping motor, which steps one step each time the flow direction is switched. The pressure from the port selected by the Scanivalve was measured by one stationary pressure transducer, made by Druck Ltd, type PDCR 22. The pressure transducer has a range of 0-6.9 kPa and an output of 17 mV at 6.9 kPa. The linearity is within ±0.06% B.S.L. Figure 4 illustrates the Scanivalve with the transducer mounted. The Scanivalve which is propelled by the compressor at 2400 RPM, has a maximum design speed of 30000 RPM.

The Pressure Blades

For the experiments, pressure taps have been made on six rotor

R Trademark of Scanivalve Inc.

blades. Each rotor blade has 5 taps with an approximate chordwise distribution of 10%, 25%, 45%, 65%, and 85%, respectively. Three blades have the taps on the pressure side and three on the suction side. Three different pairwise span distributions at 25%, 50%, and 75%, respectively, were employed. A photograph of two blades is shown in Figure 6. Altogether 30 ports were used for obtaining the blade surface pressures. The stagnation pressure was measured with a leading edge tap at the midspan radius position. Thirty-one out of 36 ports on the Scanivalve were thus used for the experiments. The pressure blades are made from ordinary RAF #6 rotor blades, with tubes mounted in milled slots and fixed with epoxy glue. The rotor blades are made of aluminum.

Description of Test Set-Up

The pressure blades were mounted pairwise in the rotor, thus, at each span position the suction side taps were facing the pressure side taps (Figure 6). The stainless steel tubes mounted in the blades were connected to the Scanivalve tubes with heat-shrinking plastic tubing, accomplishing the necessary seal. At the center of the rotor one end of a rubber hose was mounted, and the other was connected to the Scanivalve's driveshaft, employed as the propelling device for the Scanivalve. The Scanivalve was attached and centered on a support mounted on the outer housing flange. Figure 4 illustrates these arrangements.

FIGURE 6. PHOTOGRAPH OF TWO PRESSURE BLADES

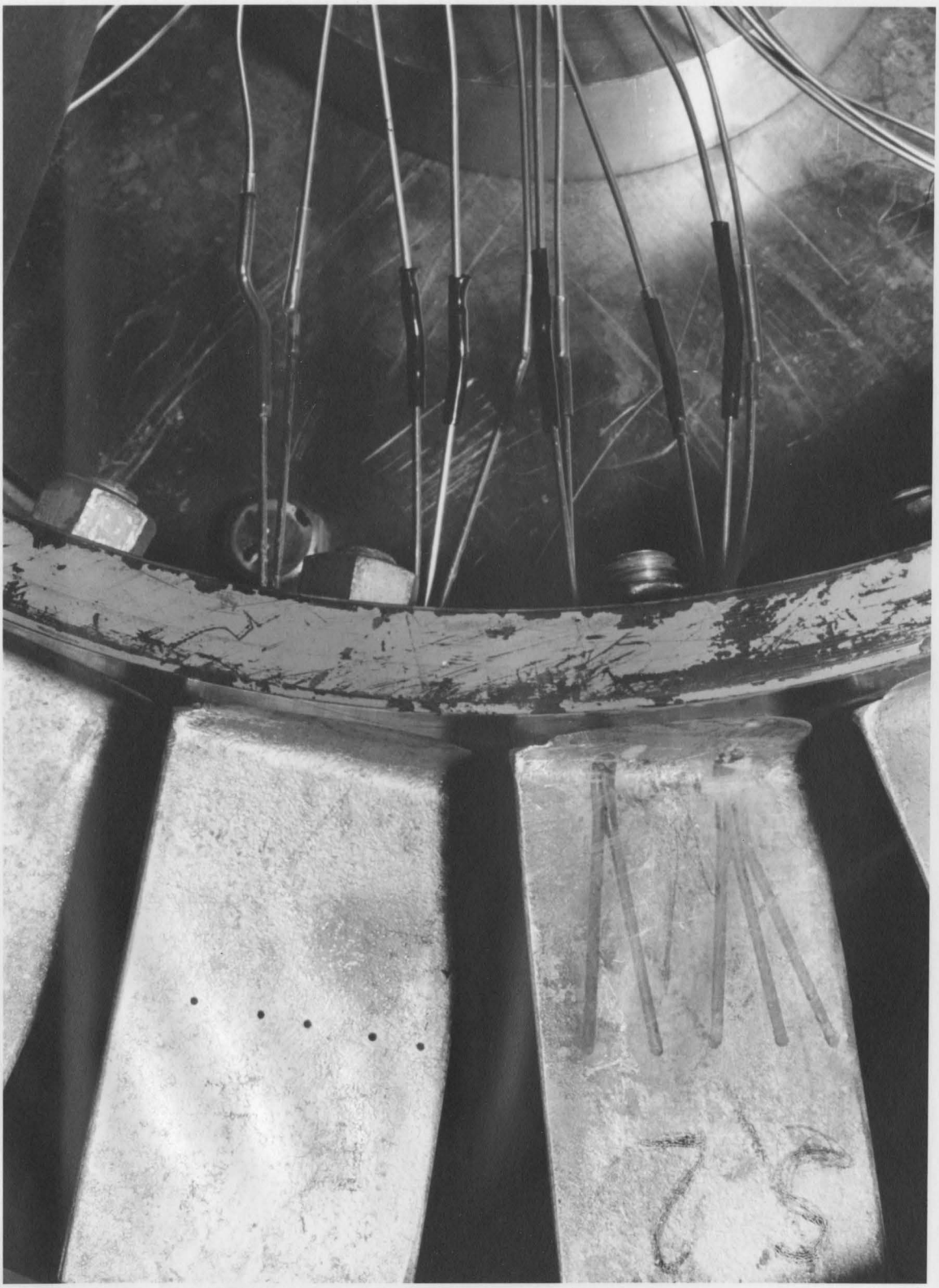

Power to the transducer was provided by a Hewlett-Packard power supply, which delivered the necessary 12 V D.C. Since the output signal from the transducer was in the range of 0-10 mV corresponding to a pressure of 0-4 kPa (0-16 inches of water), the signal was amplified to a more useful level. For this purpose a DC amplifier was connected to the pressure transducer's output and the signal was amplified to 1.5 V, corresponding to a pressure of 37 kPa (15 inches of water). A digital voltmeter with a datalogger was connected to the amplifier. The datalogger printed the data from each port. To average the fluctuating pressure signal, a low-pass filter was connected between the amplifier and the voltmeter. The low-pass filter had a 1000 μF capacitor and a 1000 Ω resistor, thus giving it a cut-off frequency of 0.16 Hz. This arrangement made it possible to read the mean pressure as a stable signal, since all frequencies above 0.16 Hz were eliminated.

Two fluidic flip-flops supplied the air-stepping motor with pressure pulses to enable selection of the desired port. The flip-flops provided signals in opposite directions, which made the Scanivalve step one step for each pulse. The pressure utilized for the pulses was approximately 500 kPa. Figure 1 is a photograph of the general set-up.

B. Test Procedure

Mean Pressure Measurements

The only compressor speed used in this investigation was 2400 RPM.

Figure 7 shows the compressor characteristic at this speed.

The blade taps were numbered from 1 to 31. One to 5 corresponded to the suction side taps and 6 to 10 to the pressure side taps at 75% span, 11 to 15 the suction side taps and 16 to 20 the pressure side taps at 50% span, 21 to 25 the suction side and 26 to 30 the pressure side taps at 25% span. Port number 31 was used for the stagnation pressure probe. The taps were connected to the corresponding tubes from the scannivalve.

The discharge valve was closed from valve position 0 to valve position 9 during the tests. Each valve position accordingly corresponded to different angles of attack (see Table 1). The angle of attack increased with increased valve position. At each valve position the surface pressure for all 30 ports was observed and printed out by the datalogger.

The pressures in front of and behind the rotor were measured during the runs. The total and static pressure were measured and the flow angle was indicated by a directional probe. The directional probe can be seen in Figure 1. This arrangement made it possible to obtain the absolute and relative velocities behind the stator and behind the rotor.

Fluctuating Pressures

Measurement of the fluctuating pressures was accomplished employing a storage-type oscilloscope. The purpose of this study was to determine the kind of fluctuations that the mean pressure measure-

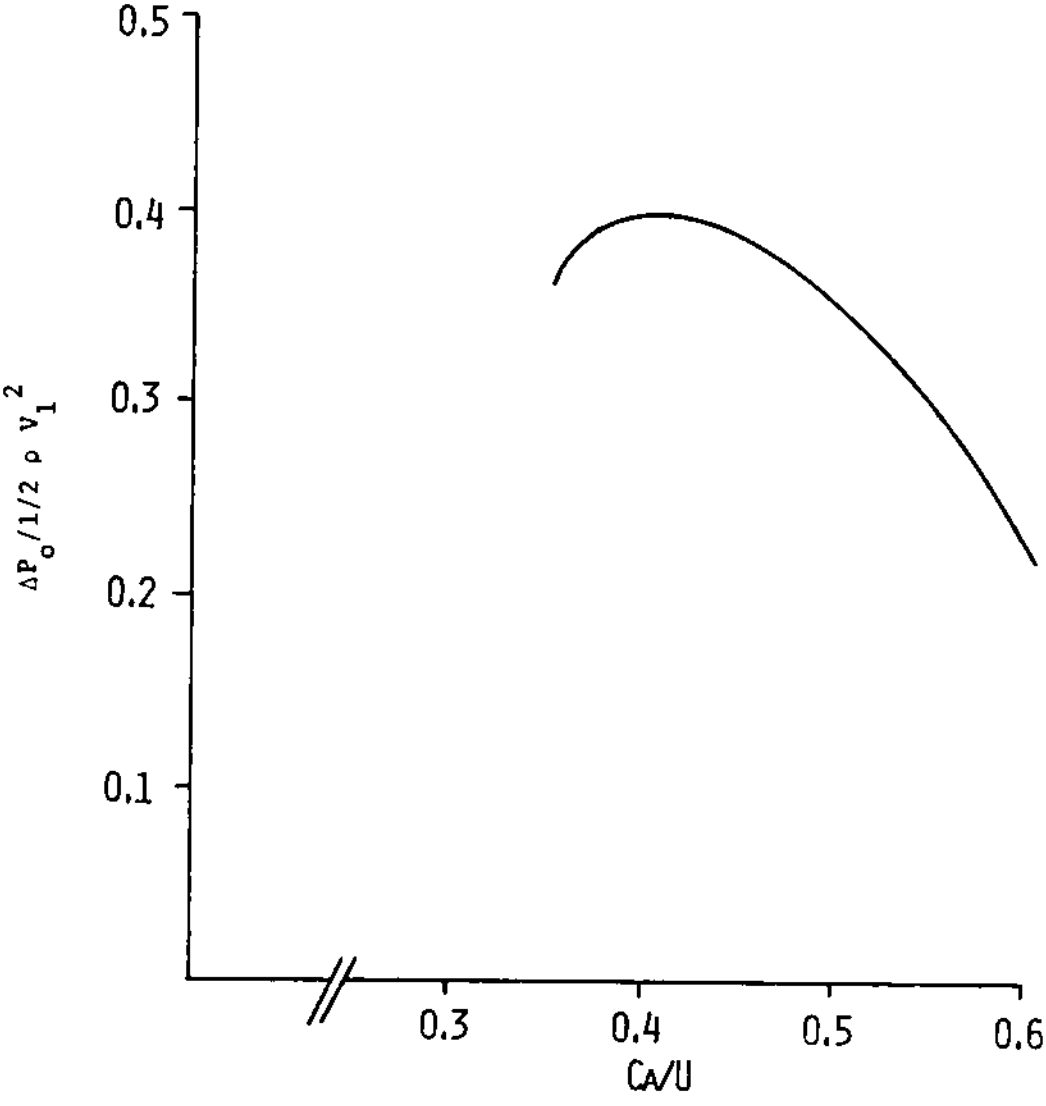

FIGURE 7. COMPRESSOR CHARACTERISTIC

ments averaged out. The nature and the reasons for the fluctuations are not investigated here. In this part of the experiments, the low-pass filter was disconnected. The same test procedure that was followed for mean pressure measurements was employed. Figure 8 shows photographs taken by a Polaroid camera during the investigation. The possible frequency response was calculated for the system. The procedure for obtaining the maximum frequency response is presented in Appendix A.

C. Evaluation of Data and Results

Pressure, Velocity Relations

The pressure data obtained from the blades were evaluated employing following procedure.

The centrifugal force acting on a rotating column of air caused a pressure difference in the measured pressure at the center of rotation from that at the blade surface. The centrifugal pressure effect was calculated by,

$$P_c = \tfrac{1}{2} \rho U^2 . \qquad (1)$$

To obtain the true surface pressure, the pressure data from the origin was thus corrected with regard to centrifugal forces.

Bernoullis equation for incompressible flow was used to relate the pressures to the velocities.

$$P_o = P + \tfrac{1}{2} \rho V^2 \qquad (2)$$

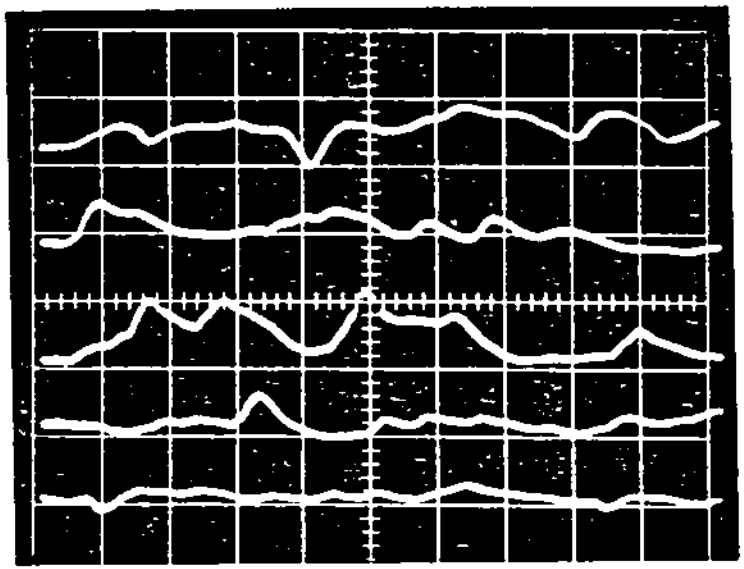

SUCTION SIDE

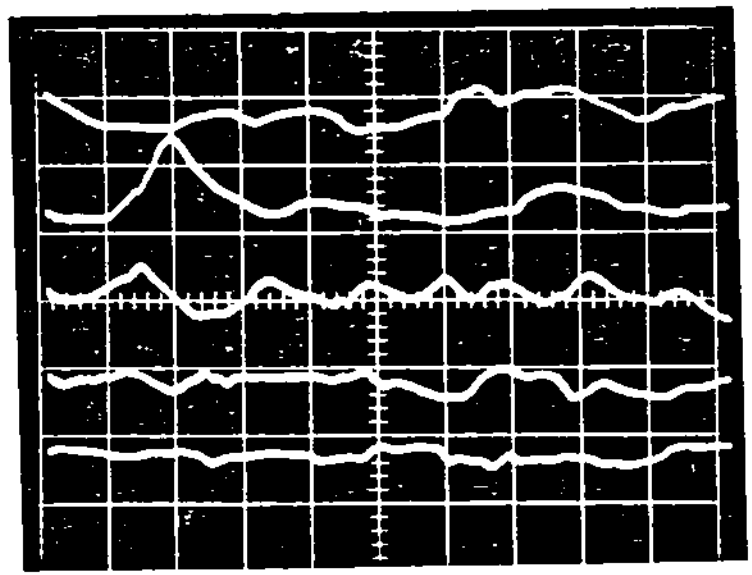

PRESSURE SIDE

VALVE POSITION 6. 10%, 25%, 45%, 65% AND 85% CHORD RESPECTIVELY.

VERTICAL SCALE 0.5 KPA/DIV. (2 INCHES OF H_2O/DIV.)

HORIZONTAL SCALE 10 MS/DIV.

FIGURE 8. FLUCTUATING PRESSURE PHOTOS

Figure 9 illustrates the relative and absolute velocities before and after the rotor.

The stagnation pressure relative to the blade P_{or} was calculated by

$$P_{or} = P_1 + \tfrac{1}{2} \rho V_1^2 \tag{3}$$

Since the total pressure relative to the rotor was assumed constant along a streamline, the static pressure at each tap P_r was related to the stagnation pressure and velocity by

$$P_{or} = P_r + \tfrac{1}{2} \rho V_r^2 \tag{4}$$

Equation 4 divided by $\tfrac{1}{2} \rho V_1^2$ yields the nondimensional pressure,

$$\left(\frac{V_r}{V_1}\right)^2 = \frac{P_{or} - P_r}{\tfrac{1}{2} \rho V_1^2} \tag{5}$$

The stagnation pressure P_{or} can be determined from two different approaches. The first approach is to use the measured value from the stagnation pressure probe on the blade. The second method is to use the data from the probe in front of the rotor. The stagnation pressure relative to the stationary probe P_{o1} was related to the absolute velocity

$$P_{o1} = P_1 + \tfrac{1}{2} \rho C_1^2 \tag{6}$$

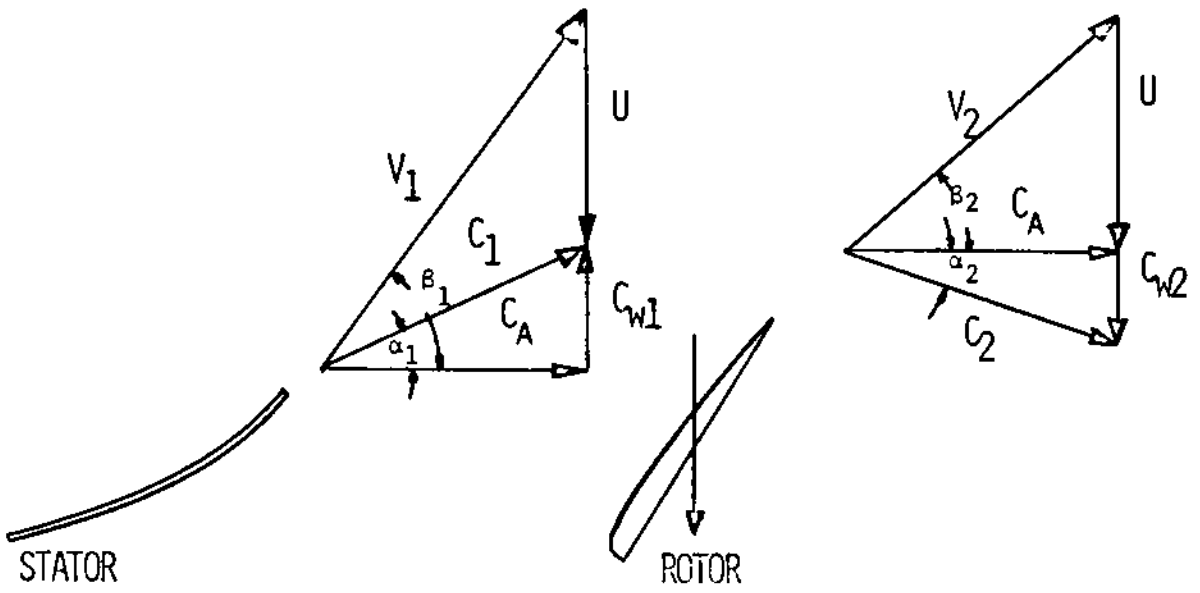

FIGURE 9. VELOCITY TRIANGLES

Equation 6 substituted into equation 3 yields

$$P_{or} = P_{ol} + \tfrac{1}{2}\rho(V_1^2 - C_1^2) \tag{7}$$

In Table 2 the results from the stationary probe are compared with the stagnation pressure obtained from the probe on the rotor blade.

Radial Equilibrium

Since the velocities and flow angles vary with radius, a method is needed to allow calculations of the velocities at any radius. The method used in this study was simple radial equilibrium. The condition of radial equilibrium was derived from the pressure balance in the radial direction.

$$(p + dp)(r + dr)d\theta - pr\,d\theta - 2(p + \frac{dp}{2})dr\,\frac{d\theta}{2} = \rho\,dr\,r\,d\theta\,\frac{C_w^2}{r} \tag{8}$$

Figure 10 illustrates equation 8. The gravitational forces have been neglected since their magnitude is insignificant compared with the centrifugal forces. All second order terms in equation 8 were neglected to obtain,

$$\frac{1}{\rho}\frac{dp}{dr} = \frac{C_w^2}{r} \tag{9}$$

Equation 9 is usually called the simple radial equilibrium condition. The derivative of equation 6 was substituted into equation 9, which gives

Table 2. Stationary-Measured versus On-Rotor-Blade Measured Stagnation Pressure

valve position	on rotor measured (inches of water)	(kPa)	stationary measured (inches of water)	(kPa)
0	7.71	(1.919)	7.77	(1.933)
1	7.61	(1.894)	7.70	(1.916)
2	7.55	(1.879	7.60	(1.891)
3	7.45	(1.854)	7.56	(1.881)
4	7.35	(1.829)	7.43	(1.889)
5	7.15	(1.779)	7.21	(1.794)
6	6.90	(1.717)	6.87	(1.710)
7	5.95	(1.481)	6.71	(1.670)
8	(4.50)	(1.120)	(7.61)	(1.894)
9	(4.70)	(1.170)	(6.63)	(1.650)

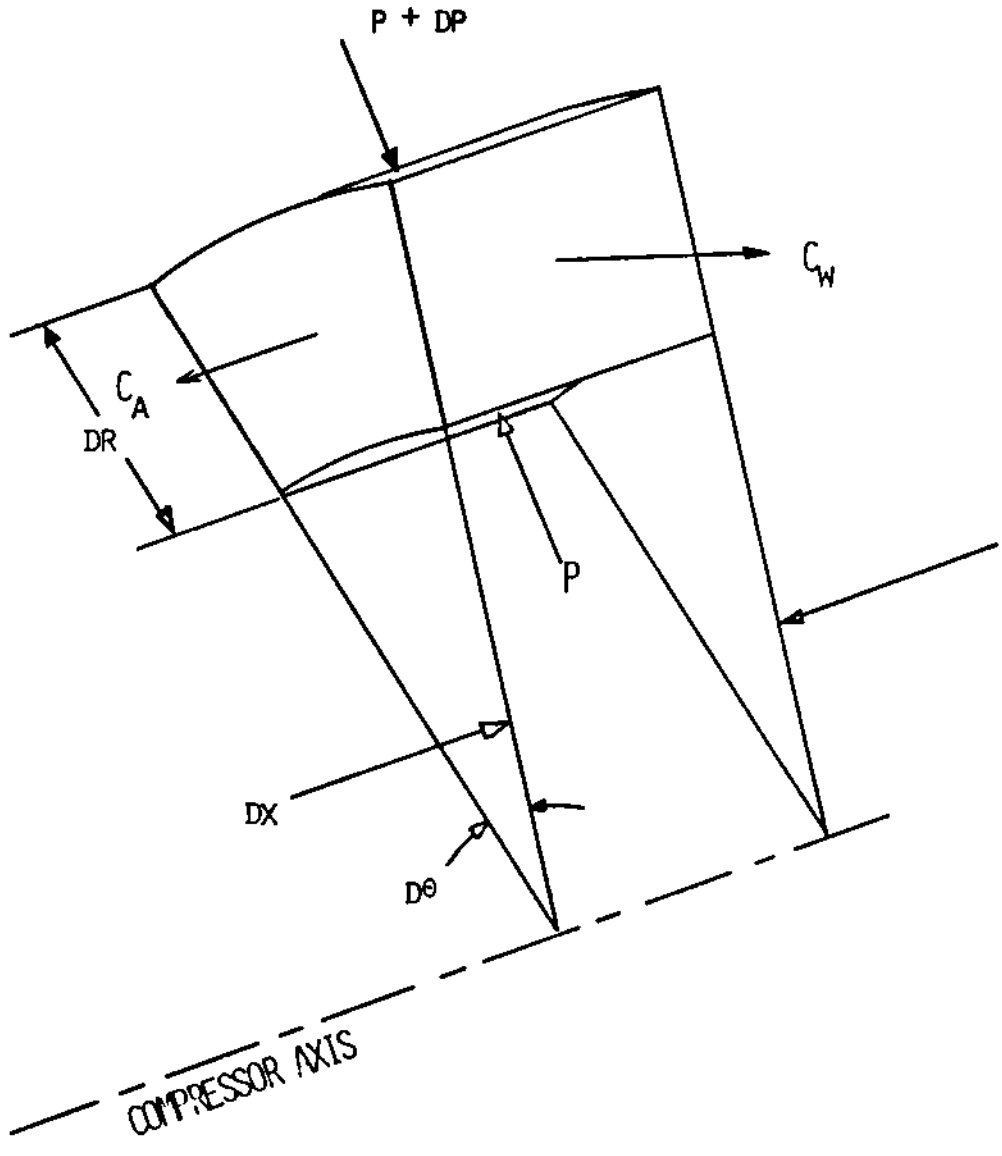

FIGURE 10. PRESSURE BALANCE FOR RADIAL EQUILIBRIUM

$$\frac{dP_{o1}}{dr} = \frac{dP_1}{dr} + \rho C \frac{dc}{dr} \tag{10}$$

From the velocity triangles, Figure 9, the trigonometric relation was obtained.

$$C^2 = C_w^2 + C_a^2 \tag{11}$$

which is differentiated to obtain

$$C \frac{dC}{dr} = C_w \frac{dC_w}{dr} + C_a \frac{dC_a}{dr} \tag{12}$$

Equation 12 combined with equation 10 yields

$$\frac{1}{\rho} \frac{dP_{o1}}{dr} = C_a \frac{dC_a}{dr} + C_w \frac{dC_w}{dr} + \frac{C_w^2}{r} \tag{13}$$

After a single stator, the stagnation pressure can be regarded as constant, that is, $\frac{dP_o}{dr} = 0$ and equation 13 becomes

$$C_a \frac{dC_a}{dr} = C_w \frac{dC_w}{dr} + \frac{C_w^2}{r} \tag{14}$$

The compressor employed in this study had a stator designed for free-vortex flow, that is, the whirl velocity C_w varies inversely with the radius. Free-vortex flow results in the axial velocity C_a constant along the radius, thus $\frac{dC_a}{dr} = 0$ and equation 14 gives

$$\frac{dC_w}{C_w} = -\frac{dr}{r} \tag{15}$$

which becomes after integration

$$C_w r = \text{constant} \tag{16}$$

Equation 16 is the free-vortex condition.

Measurements yielded a practically constant axial velocity along the radius, which justifies the assumption of constant axial velocity.

Equation 16 yields a blade twist of 8 degrees on the stator, which also was the twist on the stator employed for the experiments.

The pressures and angles obtained from a pressure probe in front of and behind the rotor are tabulated in Table 3 of Appendix B. Table 4, 5, and 6 shows the velocities derived from Table 3 and radial equilibrium.

It was also investigated whether or not the measured mean pressure was the true average pressure. The only part of the experiments where this procedure was required was in the region of larger pressure fluctuations, essentially valve position 5 through 9. Reference 8 presents an investigation of oscillating pressures. On the compressor employed in this study, the difference between the highest and the lowest pressure was about 0.5 kPa (2 inches of water), which made a maximum versus minimum pressure ratio of 1.05. The total error of the measured pressure versus the true pressure should be with this ratio, according to reference 8, significantly less than 1%. Figure 8 shows photographs of the fluctuating pressure.

The results of the non-dimensionalized chordwise pressure distribution at 25%, 50%, and 75% span obtained in the experiments are

presented in Figure 12a through j. The symbols used in these figures are given in Figure 11.

Part 2

A. Analytical Investigation

Computer Program

Air, which is to be regarded as a Newtonian fluid, is governed by; the continuity equation 20, the Navier-Stokes equations 21, the energy equation 22, and the thermal and caloric equations of state 23.

$$\frac{\partial P}{\partial t} + \frac{\partial}{\partial x_k}(\rho u_k) = 0 \tag{20}$$

$$\rho \frac{\partial u_j}{\partial t} + \rho u_k \frac{\partial u_j}{\partial x_k} = - \frac{\partial P}{\partial x_j} + \frac{\partial}{\partial x_j}(\lambda \frac{\partial u_k}{\partial x_k}) + \frac{\partial}{\partial x_i}[\mu(\frac{\partial u_i}{\partial x_j} + \frac{\partial u_j}{\partial x_i})] + \rho f_i \tag{21}$$

$$\rho \frac{\partial e}{\partial t} + \rho u_k \frac{\partial e}{\partial x_k} = - P \frac{\partial u_k}{\partial x_k} + \frac{\partial}{\partial x_j}(k \frac{\partial T}{\partial x_j}) + \lambda(\frac{\partial u_k}{\partial x_k})^2 + \mu(\frac{\partial u_i}{\partial x_j} + \frac{\partial u_j}{\partial x_i})\frac{\partial u_j}{\partial x_i} \tag{22}$$

$$\left.\begin{aligned} P &= P(\rho, T) \\ e &= e(\rho, T) \end{aligned}\right\} \tag{23}$$

e represents the internal energy per unit mass in these equations.

Since the equations are coupled and nonlinear, assumptions must be made to obtain a solution.

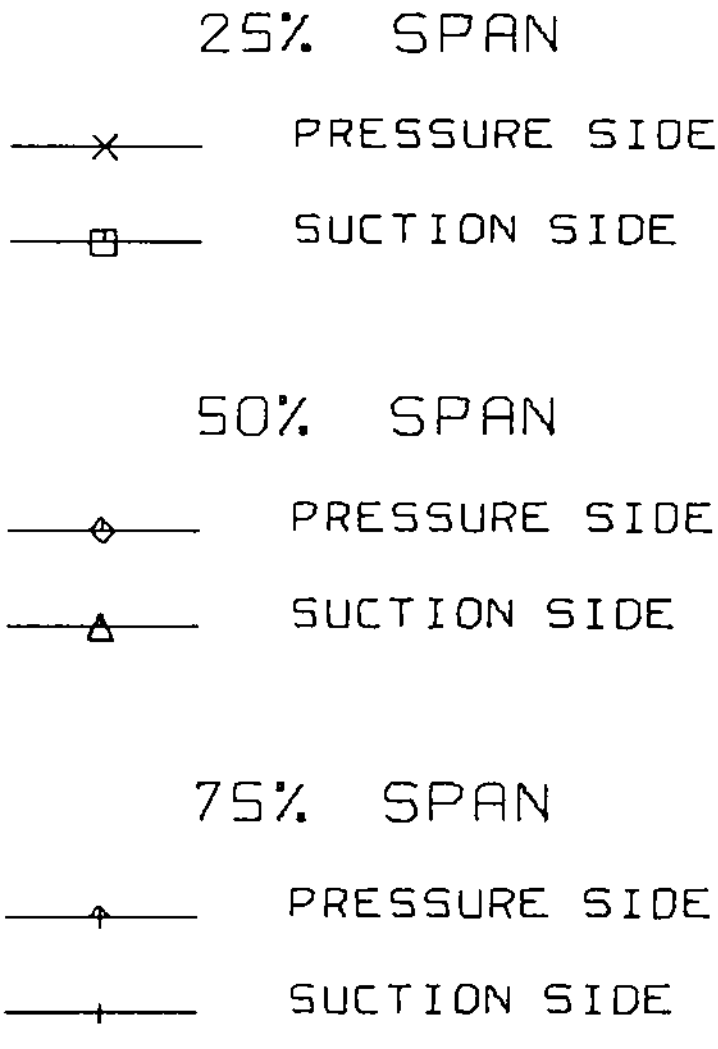

FIGURE 11. SYMBOLS USED IN FIG. 12

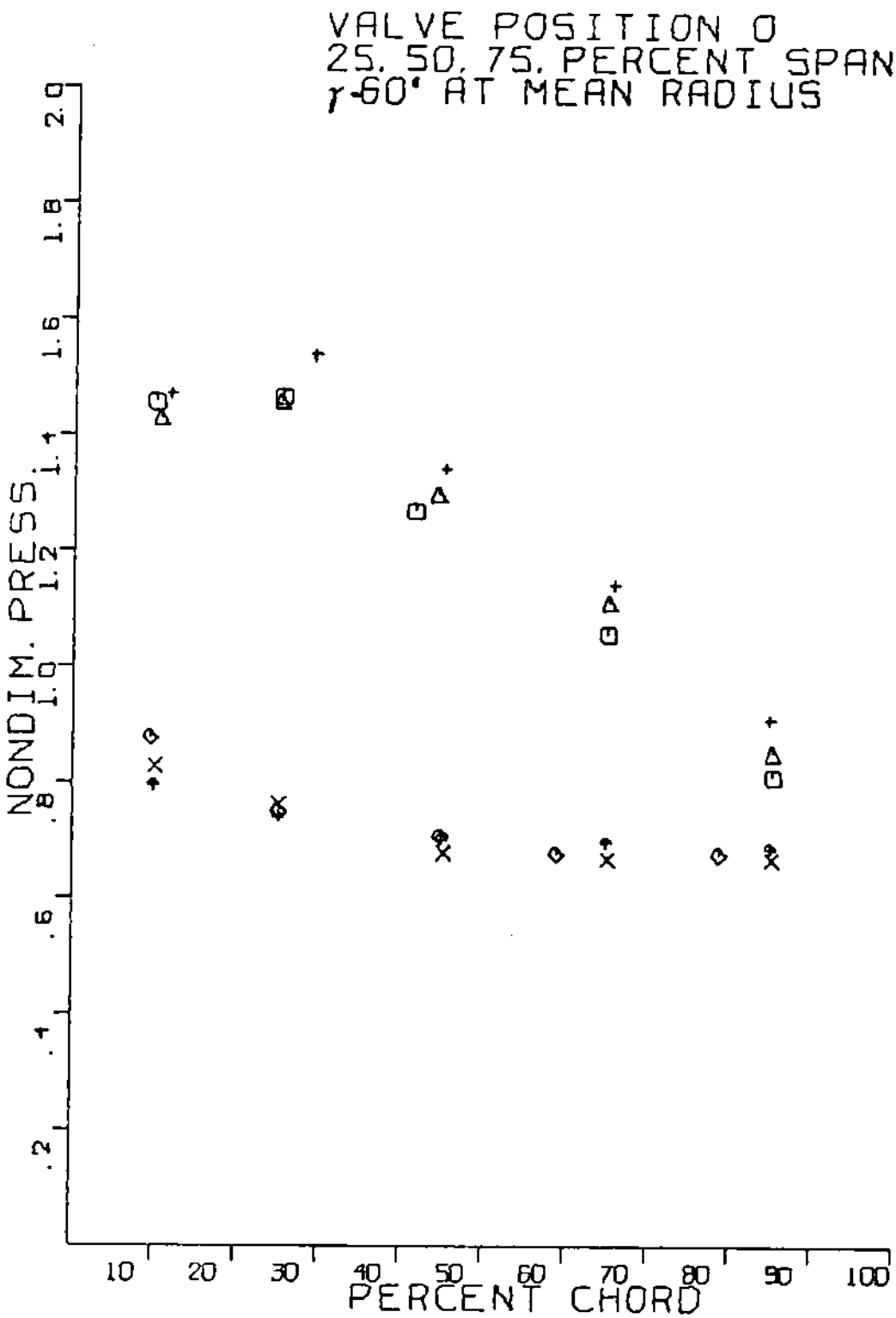

FIGURE 12a EXPERIMENTAL NONDIM. PRESSURE DISTRIBUTION

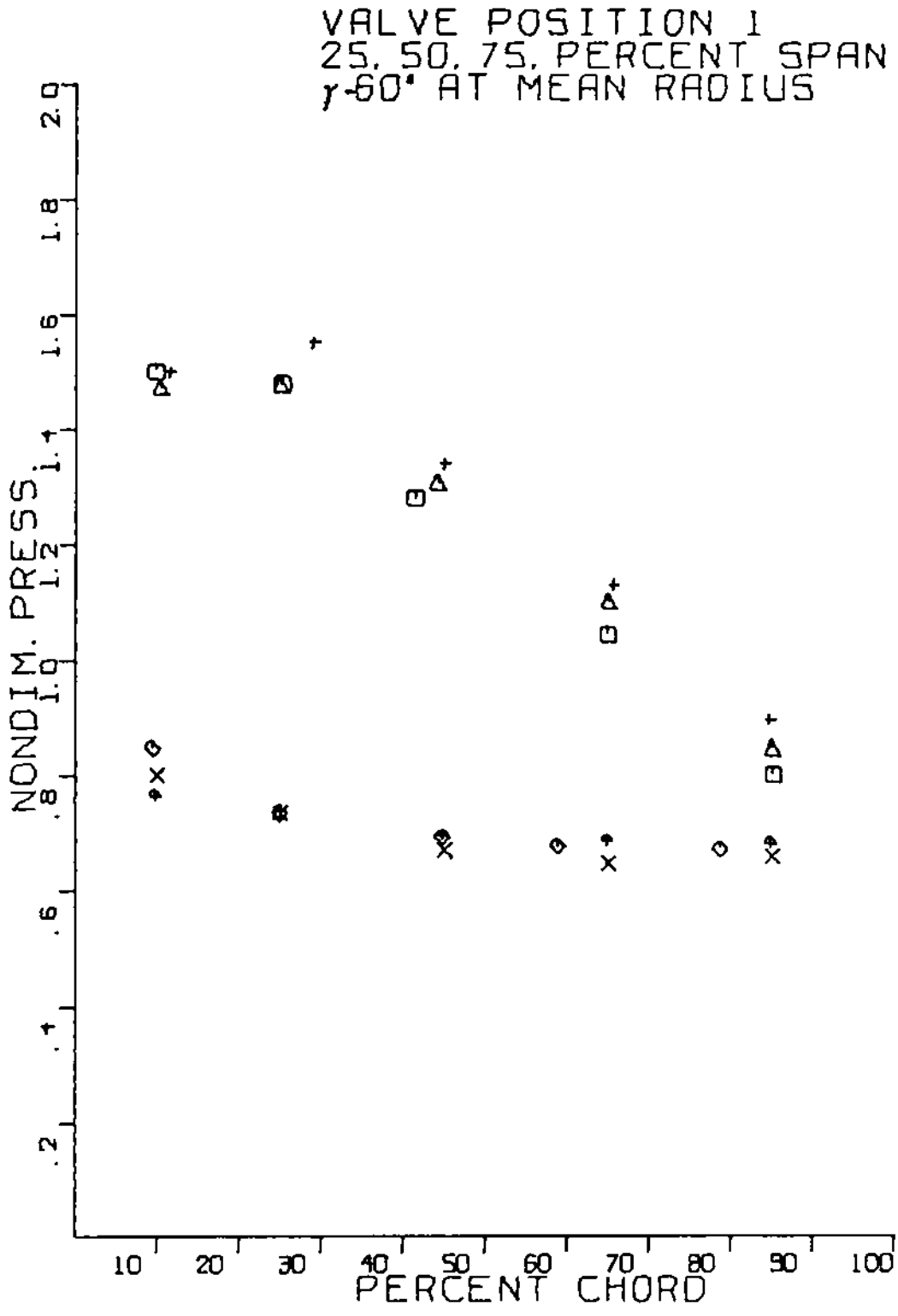

FIGURE 12b EXPERIMENTAL NONDIM. PRESSURE DISTRIBUTION

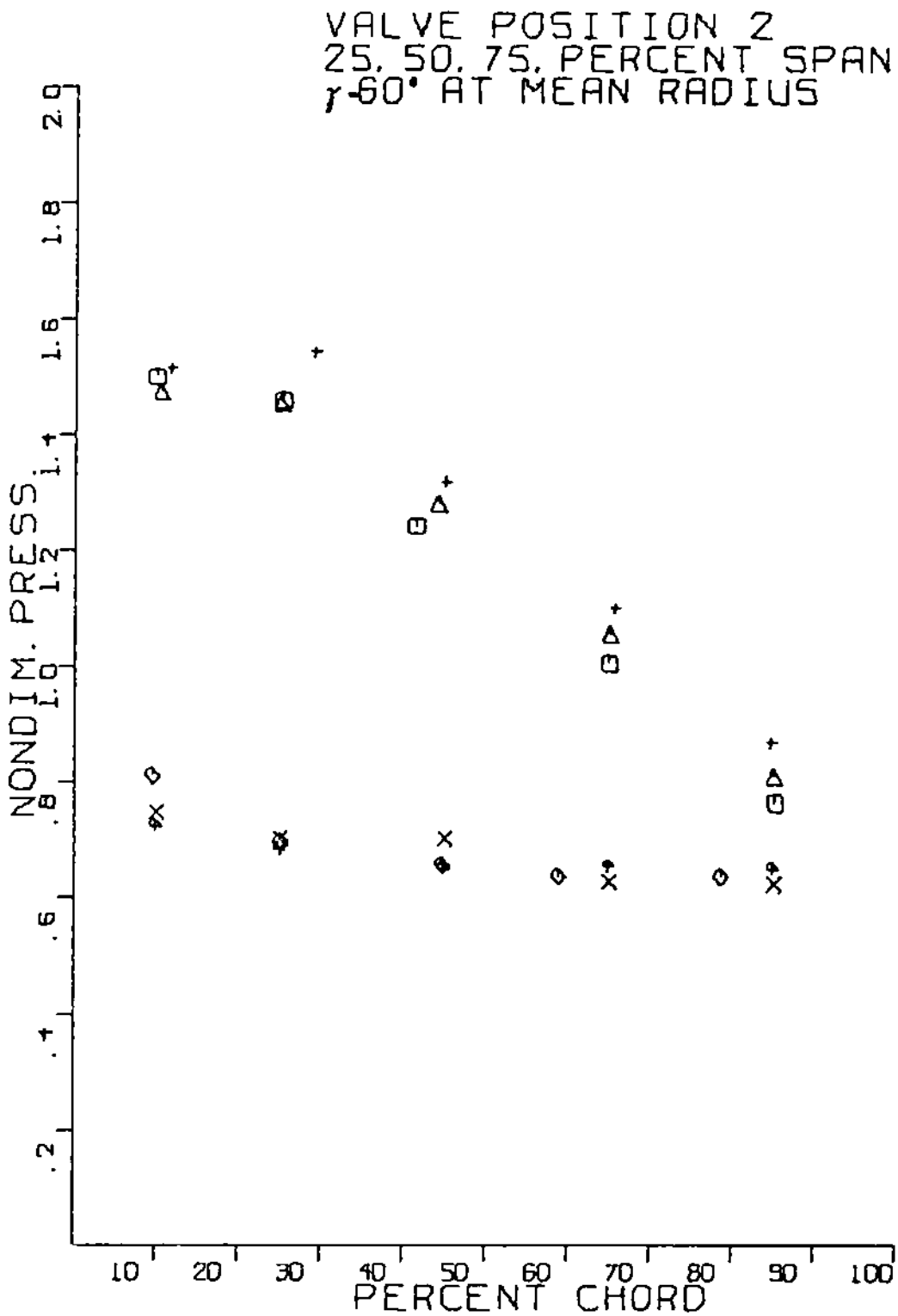

FIGURE 12c EXPERIMENTAL NONDIM. PRESSURE DISTRIBUTION

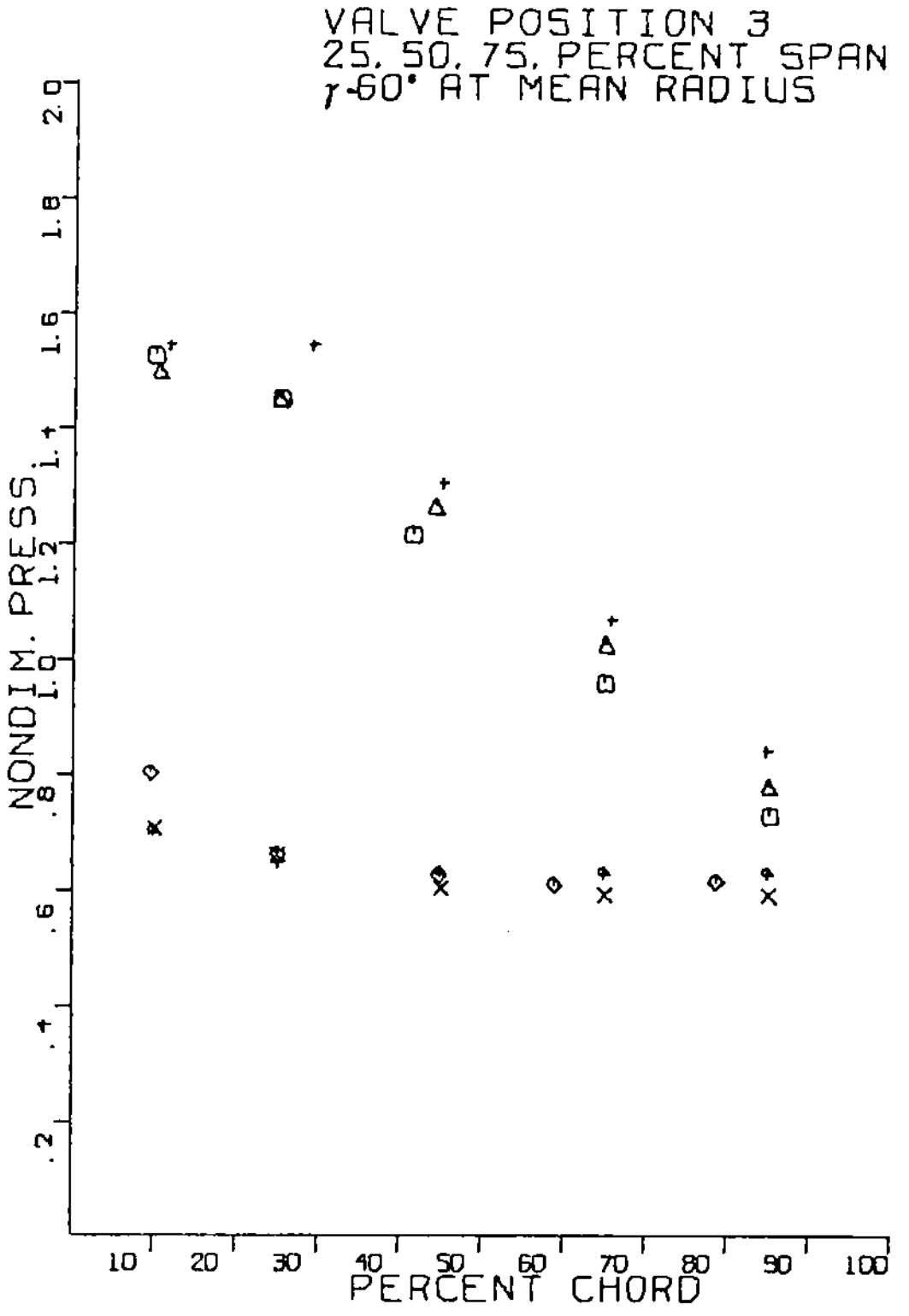

FIGURE 12d EXPERIMENTAL NONDIM. PRESSURE DISTRIBUTION

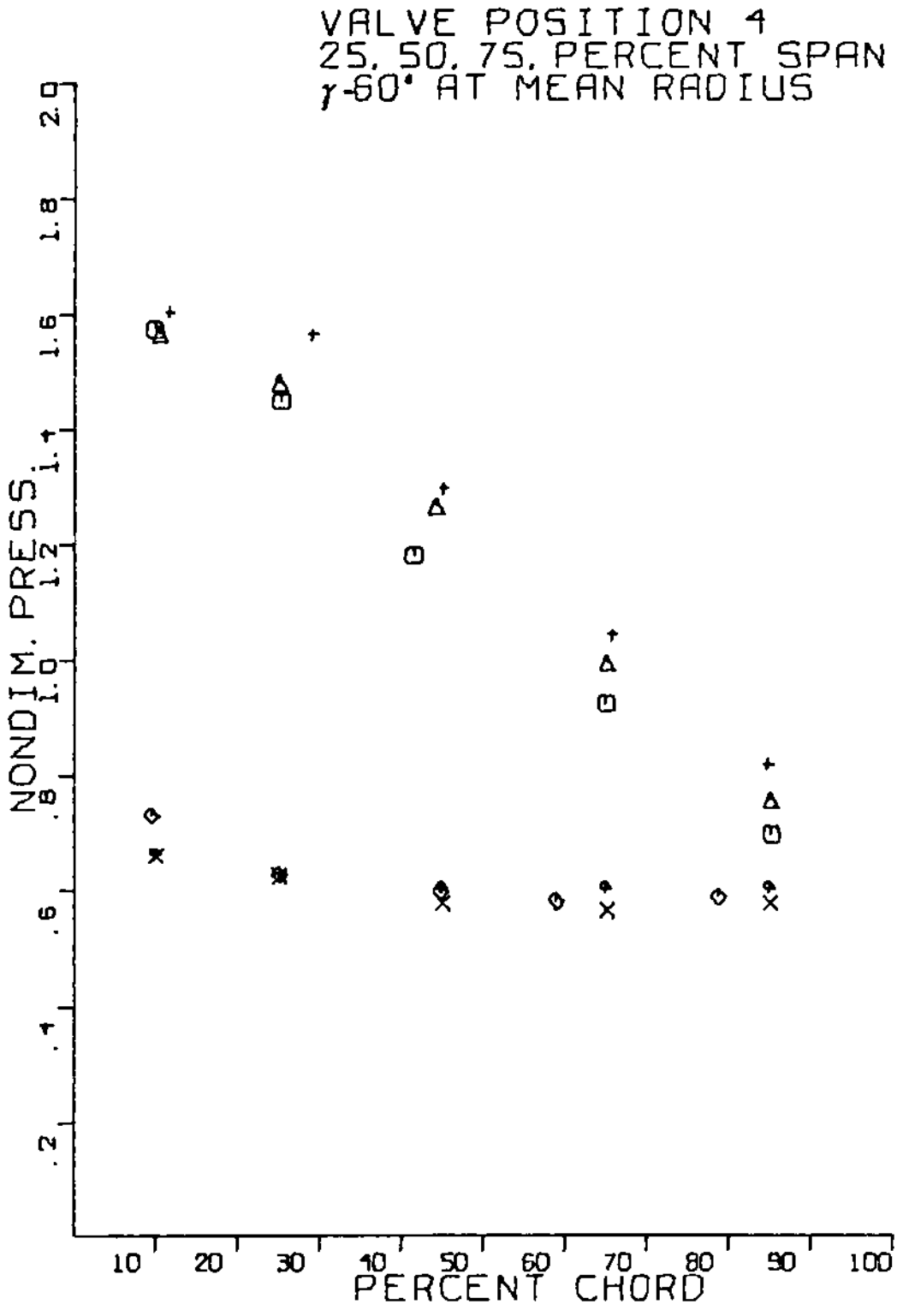

FIGURE 12e EXPERIMENTAL NONDIM. PRESSURE DISTRIBUTION

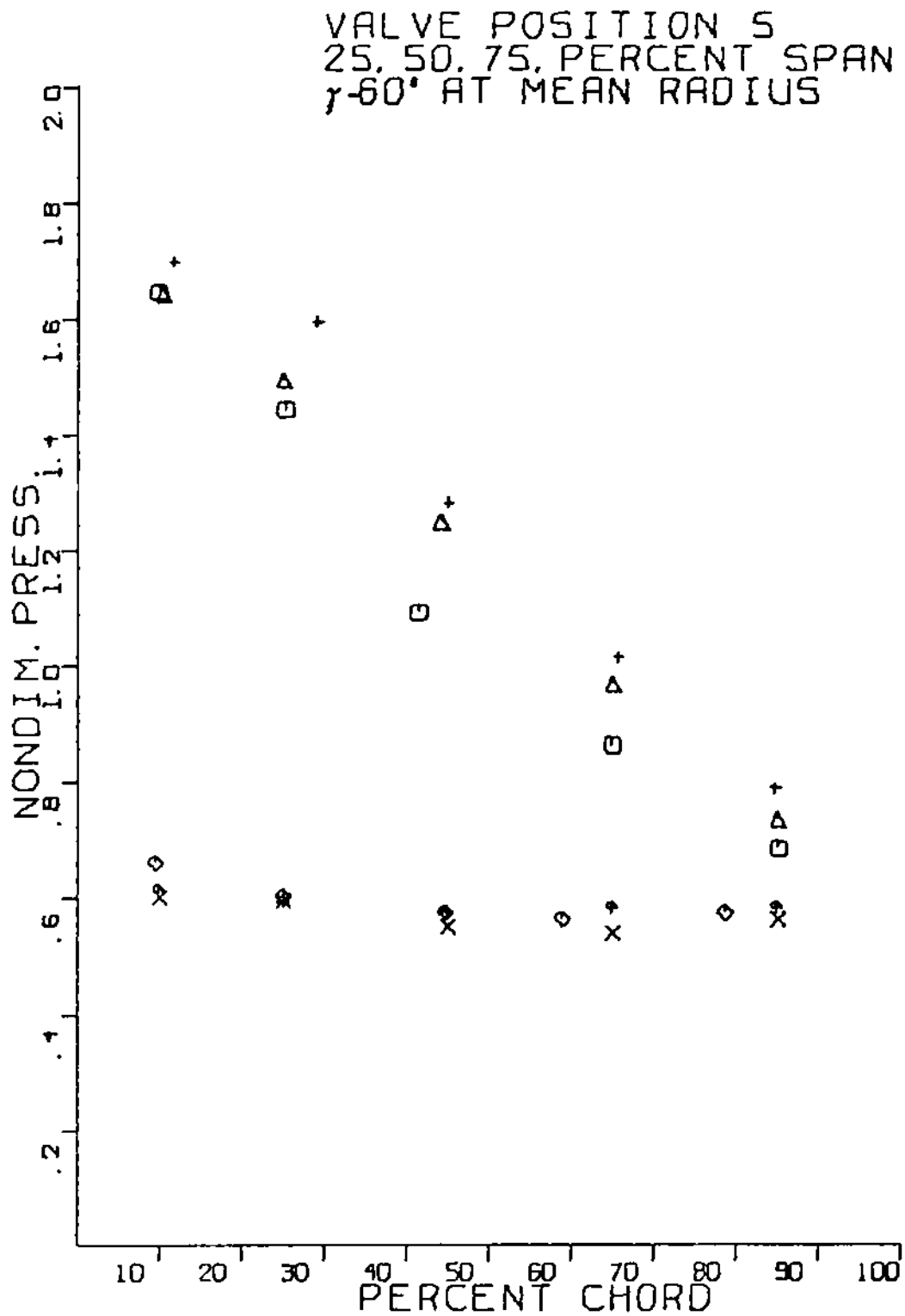

FIGURE 12f EXPERIMENTAL NONDIM. PRESSURE DISTRIBUTION

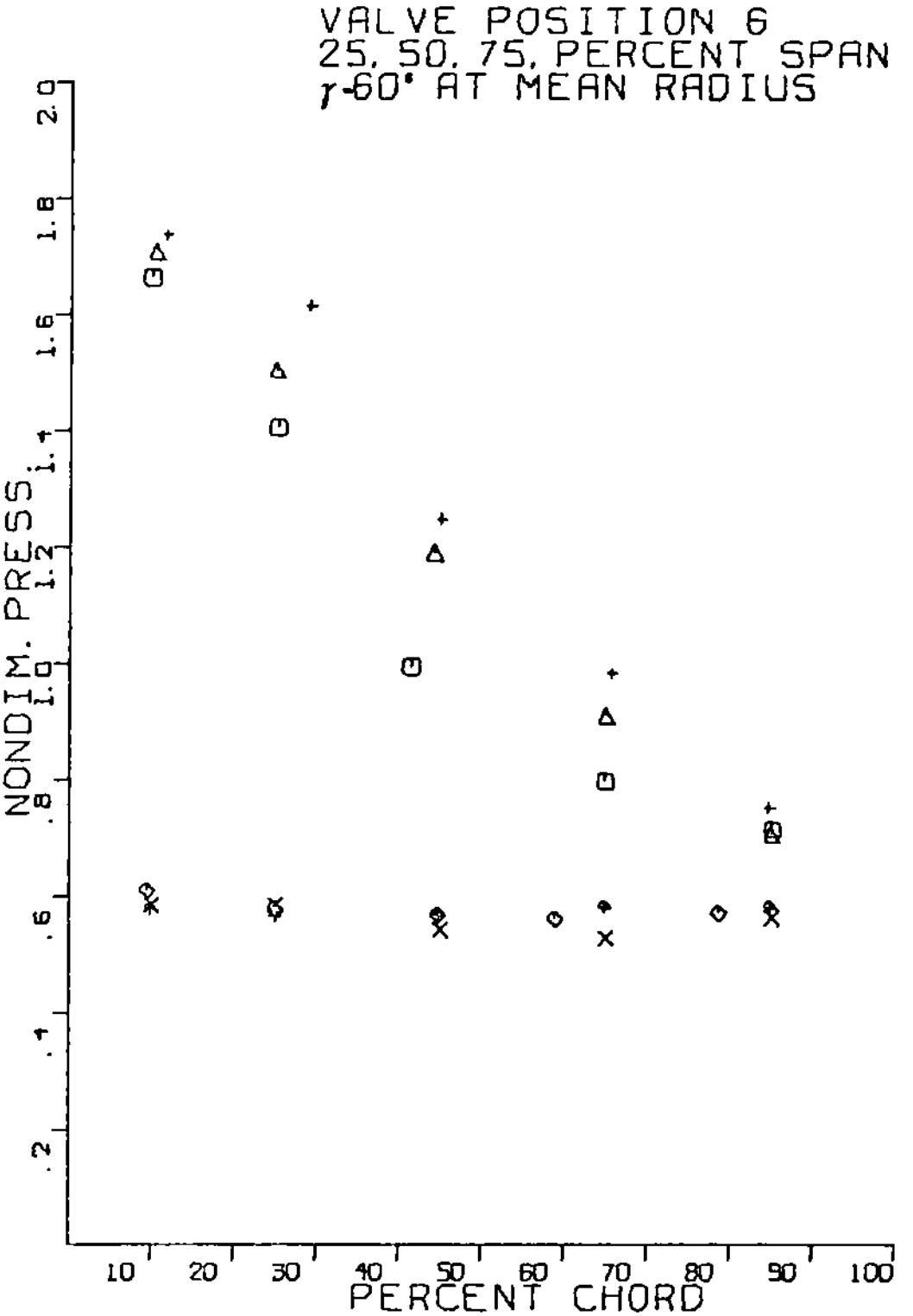

FIGURE 12g EXPERIMENTAL NONDIM. PRESSURE DISTRIBUTION

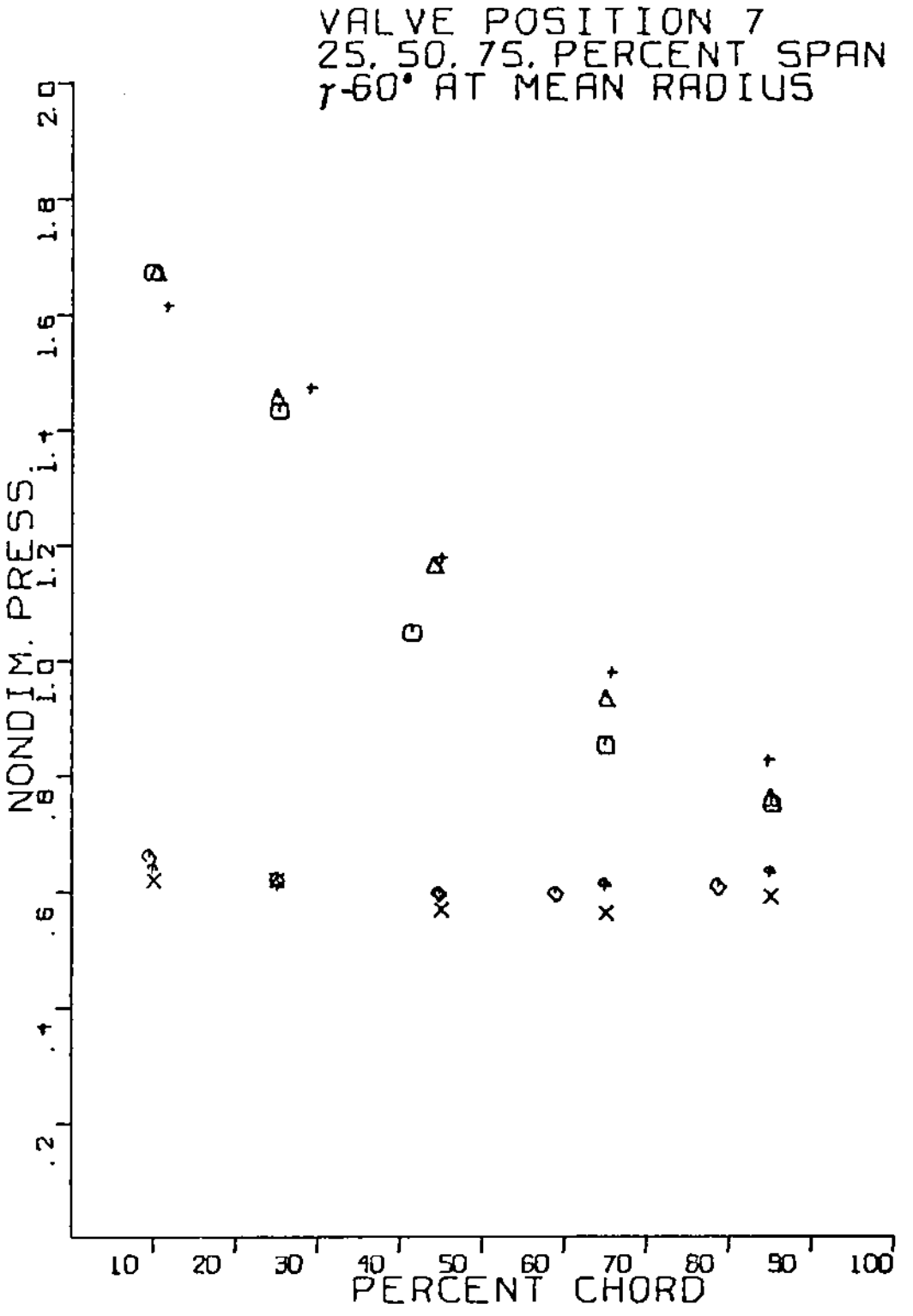

FIGURE 12h EXPERIMENTAL NONDIM. PRESSURE DISTRIBUTION

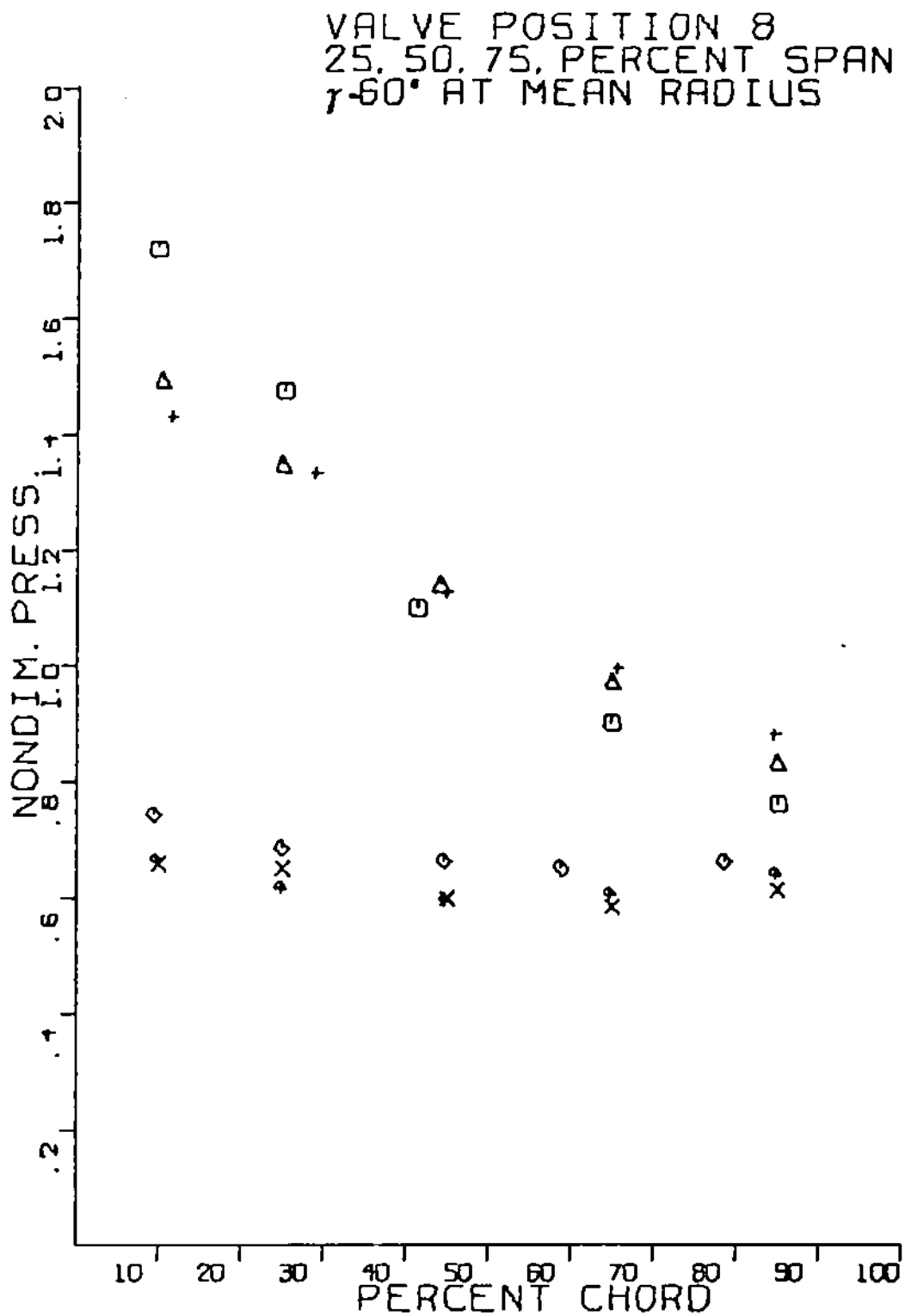

FIGURE 12i EXPERIMENTAL NONDIM. PRESSURE DISTRIBUTION

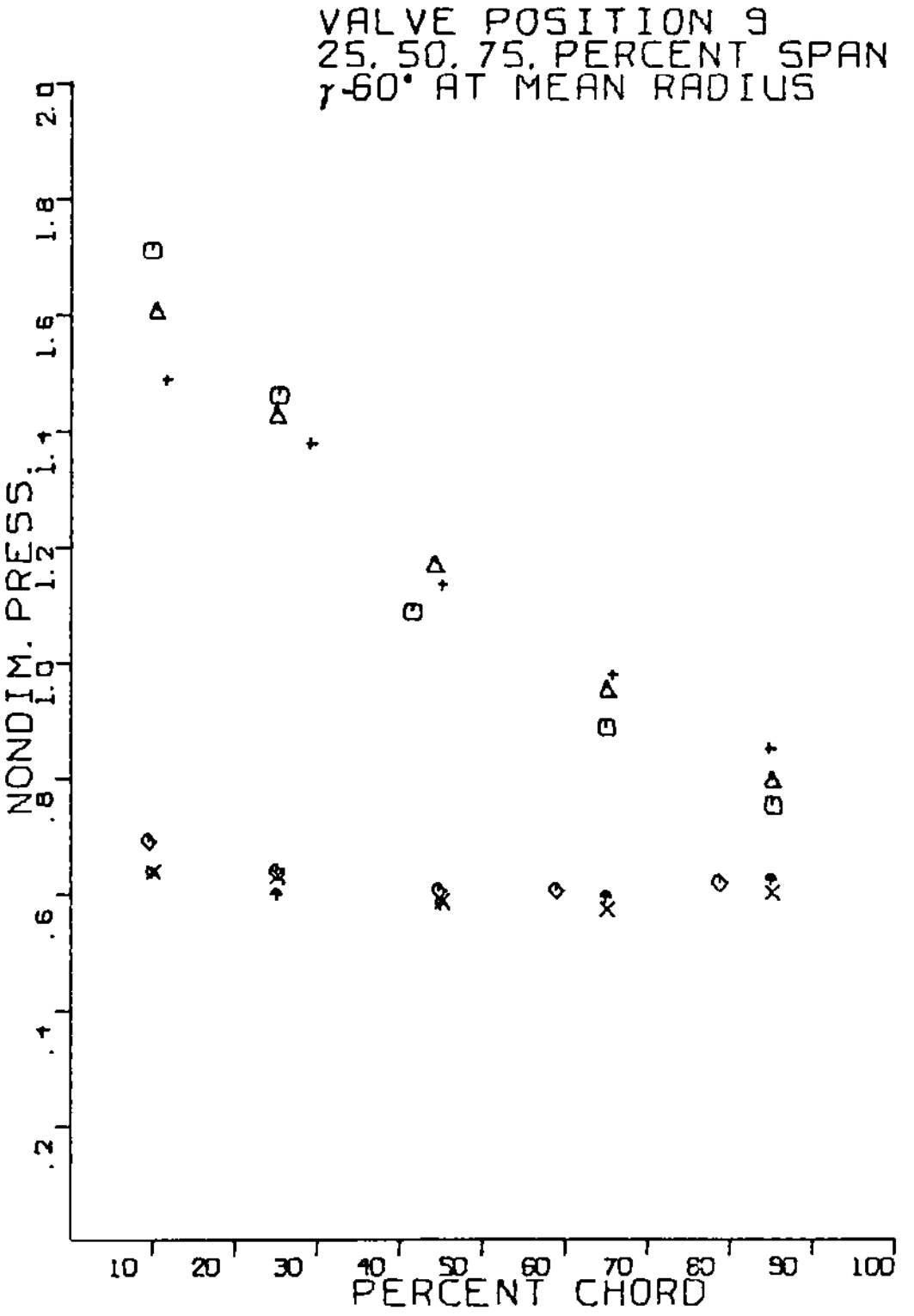

FIGURE 12j EXPERIMENTAL NONDIM. PRESSURE DISTRIBUTION

1. The flow is considered incompressible.

This assumption uncouples the energy equation 22 from the continuity equation 20 and Navier-Stokes equations 21. This has the advantage that it now is possible to solve for the velocities and pressures without reference to the energy equation. Furthermore if equation 20 is expanded to the form

$$\frac{\partial \rho}{\partial t} + u_k \frac{\partial \rho}{\partial x_k} + \rho \frac{\partial u_k}{\partial x_k} = 0, \tag{20b}$$

it is seen that the two first terms in 20b are due to compressibility and thus equal to zero, hence equation 20b yields

$$\frac{\partial u_k}{\partial x_k} = 0. \tag{24}$$

2. Negligible viscous effects.

With this assumption, the Navier-Stokes equations 21 becomes,

$$\rho \frac{\partial u_j}{\partial t} + \rho u_k \frac{\partial u_j}{\partial x_k} = - \frac{\partial P}{\partial x_j} + \rho f_j. \tag{21b}$$

The two equations left now, 24 and 21b, are the equations governing the velocity and pressure fields for an ideal fluid.

For a two-dimensional flow the continuity equation becomes in Cartesian coordinates 25 and the two components of the Navier-Stokes equations 26.

$$\frac{\partial u}{\partial x} + \frac{\partial v}{\partial y} = 0 \tag{25}$$

$$\left.\begin{aligned} \frac{\partial u}{\partial t} + u\frac{\partial u}{\partial x} + v\frac{\partial u}{\partial y} &= -\frac{1}{\rho}\frac{\partial P}{\partial x} + g_x \\ \frac{\partial v}{\partial t} + u\frac{\partial v}{\partial x} + v\frac{\partial v}{\partial y} &= -\frac{1}{\rho}\frac{\partial P}{\partial x} + g_y \end{aligned}\right\} \tag{26}$$

To eliminate the gravity and pressures from the two equations 25 and 26, they are cross-differentiated, which yields,

$$\frac{\partial}{\partial t}\left(\frac{\partial v}{\partial x} - \frac{\partial u}{\partial y}\right) + u\frac{\partial}{\partial x}\left(\frac{\partial v}{\partial x} - \frac{\partial u}{\partial y}\right) + v\frac{\partial}{\partial y}\left(\frac{\partial v}{\partial x} - \frac{\partial u}{\partial y}\right) = 0. \tag{27}$$

Inside the parenthesis is the definition of the vorticity w in the z-direction

$$w_z = \frac{\partial v}{\partial x} - \frac{\partial u}{\partial y}\,. \tag{28}$$

3. The flow is irrotational.

The condition of irrotationality for a two-dimensional flow is $w_z = 0$ which yields

$$\frac{\partial v}{\partial x} - \frac{\partial u}{\partial y} = 0. \tag{29}$$

The governing equations for the flow are now simplified enough that it is possible to obtain a solution for the flow field. This solution is called the potential flow solution.

Introducing the stream function ψ, which is defined by the following,

$$u = \frac{\partial \psi}{\partial y} \quad \text{and} \quad v = -\frac{\partial \psi}{\partial x} \tag{30}$$

Equation 30 is substituted into equation 29 and the Laplace's equation for the stream function is obtained.

$$\frac{\partial^2 \psi}{\partial x^2} + \frac{\partial^2 \psi}{\partial y^2} = 0 \tag{31}$$

The stream function satisfies the continuity equation 25.

$$\frac{\partial^2 \psi}{\partial x \, \partial y} - \frac{\partial^2 \psi}{\partial y \, \partial x} = 0$$

Two useful properties of the stream function are to be mentioned here.

1. Lines where ψ is constant are the stream lines of the flow field.
2. The different values of two stream lines gives the volume of the fluid which is flowing between these two stream-lines.

The computer program utilized in this study essentially solves the Laplace's equation for the stream function 31 everywhere in the flow field. The area of interest is between two adjacent rotor blades.

To solve equation 31 with a computer, a numerical method must be used. The method employed in this investigation was a finite difference method.

$$\frac{\partial^2\psi}{\partial x^2} + \frac{\partial^2\psi}{\partial y^2} = \frac{\dfrac{\psi_4 - \psi_1}{\Delta x_2} - \dfrac{\psi_1 - \psi_2}{\Delta x_1}}{\frac{1}{2}(\Delta x_1 + \Delta x_2)} + \frac{\dfrac{\psi_3 - \psi_1}{\Delta y_2} - \dfrac{\psi_1 - \psi_5}{\Delta y_1}}{\frac{1}{2}(\Delta y_1 + \Delta y_2)} = 0$$

The finite difference method is illustrated in Figure 13.

Owing to the fact that Laplace's equation is elliptic by nature, it is a boundary value problem, and it was thus necessary to apply boundary conditions on a "complete contour enclosing the region." Figure 14 illustrates the area of investigation. The boundary conditions used in the computer program are briefly described here.

The stream function ψ was assumed constant along the blade surfaces. ψ was set to 1 on the upper surface IK and equal to 0 on the lower surface HJ. In the area ABC upstream of the rotor, the flow was assumed uniform. ψ_A was calculated each iteration and ψ_B was set $\psi_A + 1$. The intersection point of the streamline upstream from B and AC thus had the value $\psi_A + 1$. Accordingly AC was divided uniformly and all points given corresponding values. CB achieved values in a similar way. The line AH was calculated and BI was given one unit higher values. At each iteration AH and BI changed values but added or subtracted one unit corresponding to their position. In a similar way the area downstream of JK obtained values. Hence the boundary conditions were determined. All points within the area ACEF were given arbitrary initial values.

The procedure that the program employs to calculate values for each point within the area ACEF is the Gauss-Seidel method. In the

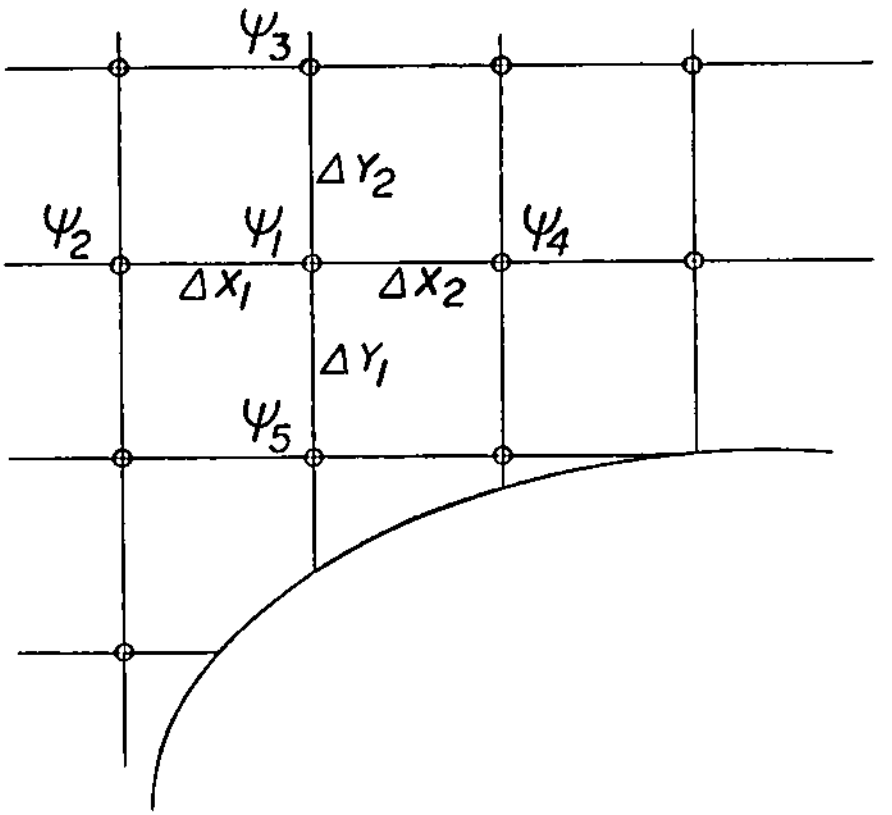

FIGURE 13. COMPUTATIONAL MOLECULE

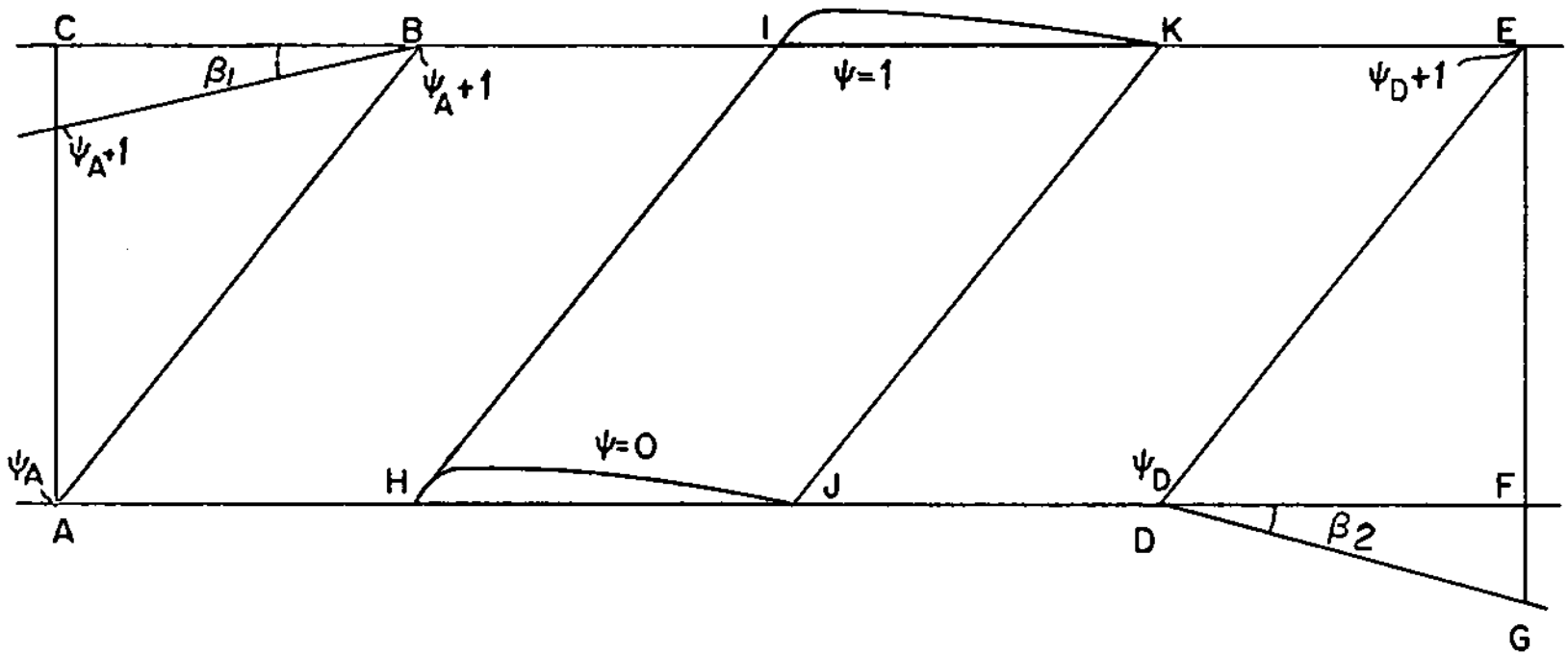

FIGURE 14. AREA OF INVESTIGATION IN THE COMPUTER PROGRAM

iteration procedure calculating the center point ψ_1 (Figure 13), the values for ψ_3 and ψ_4 were from the previous iteration, while the recently obtained values for ψ_2 and ψ_5 were used. The "computational molecule" stepped ahead so that ψ_3 became ψ_1 and used the recently calculated data and "old" values to achieve a value for the new ψ_1 and so on. After a large number of iterations the change between the old value and the new value was sufficiently small and the execution ended.

The two input variables in the program were the inlet velocity angle β_1 and the outlet velocity angle β_2. β_1 was given the desired angle and for each β_1 the angle β_2 was changed until the trailing edge condition was satisfied.

The trailing edge condition, in this case was the Kutta condition since the flow was assumed inviscid. The Kutta condition [16] requires that the velocities and hence the pressures on the pressure and suction surfaces be equal at the trailing edge. Figure 15a and b illustrates the determination of the Kutta condition.

Boundary Layer

Since an exact solution to the governing equations 20 through 23 has not yet appeared, an approximation to simulate viscous flow must be used. The method used here was to assume that the effects of viscosity were concentrated in a thin strip adjacent to the blade surface, and the flow outside of this narrow region was regarded as irrotational. This thin layer on the blade surface is called the

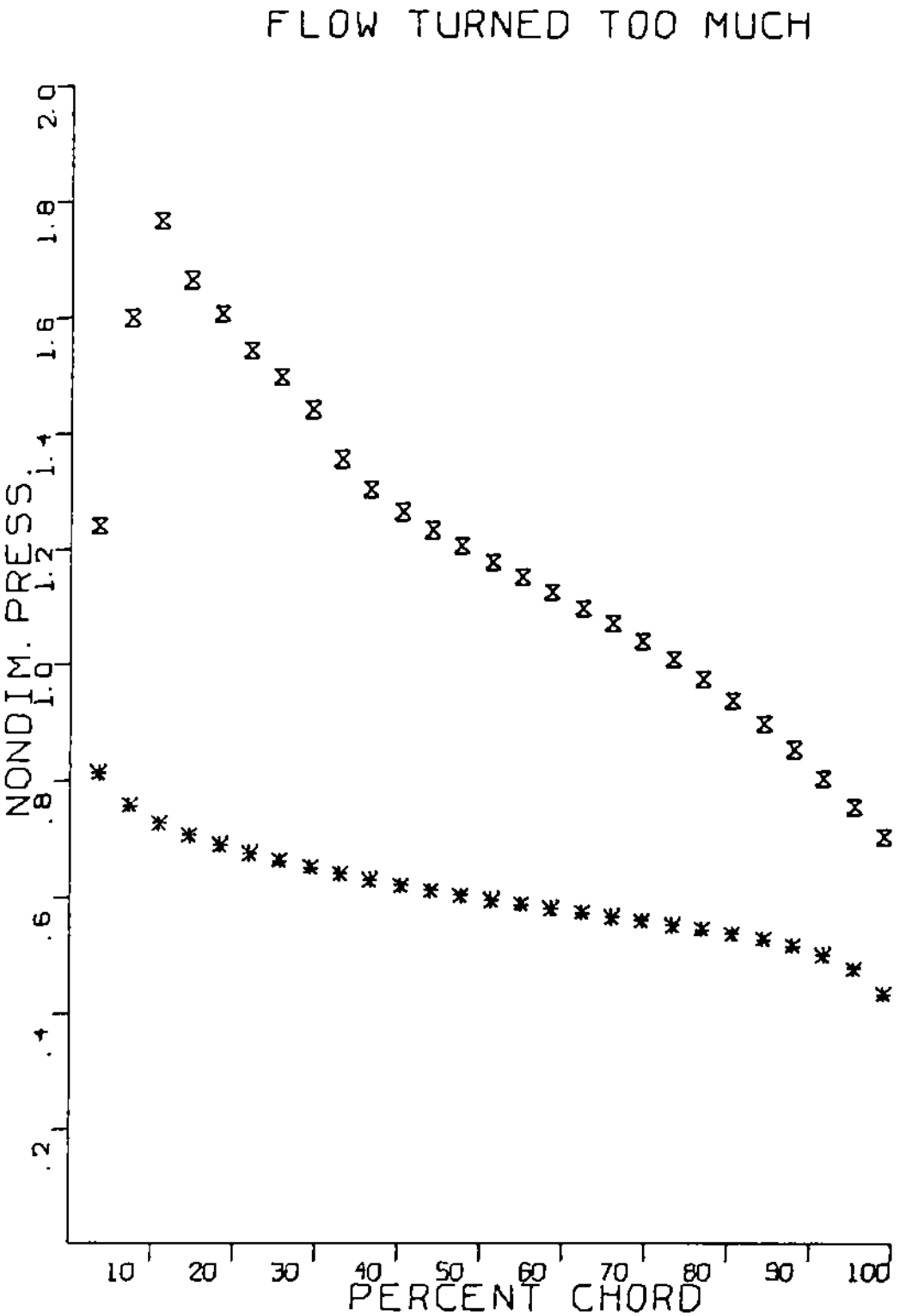

FIGURE 15a. DETERMINATION OF THE TRAILING EDGE CONDITION

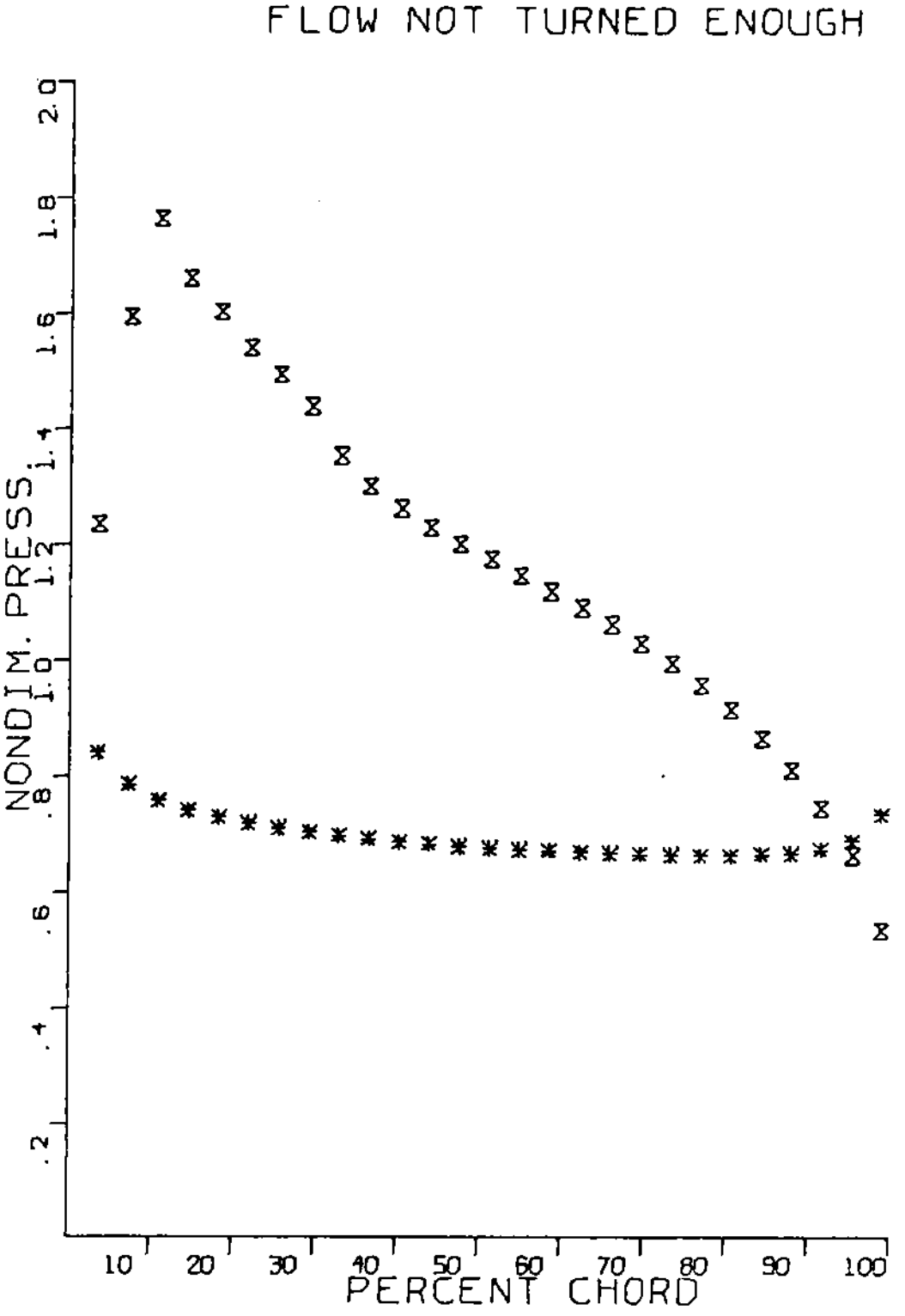

FIGURE 15b, DETERMINATION OF THE TRAILING EDGE CONDITION

boundary layer. To be able to calculate the boundary layer, information about the surface velocities was necessary. If the boundary layers are thin the velocity distribution obtained from potential flow calculations earlier is a good approximation. In reference 11, Bryner has calculated the boundary layer along the blade suction surface. From these calculations the displacement thickness distribution over the blade surface suction side was obtained as a function of the chord length. A polynomial fitted to the displacement thickness allowed substitution for the blade surface in the computer program.

For the pressure side displacement thickness distribution, the flat plate approach was used, since the pressure on this side was essentially uniform. Appendix C describes the procedure used to calculate the displacement thickness on the pressure side. Figure 16 illustrates the boundary layer displacement thicknesses. The wake after the trailing edge was approximated in the computer program by adding a source at the trailing edge, that is, increase the size of the stream function at the trailing edge. Since the pressure distribution did not change a large amount with the angle of attack, the same approximation for the boundary layer was used in all cases. In Appendix D the computer program employed in this study is listed.

B. Results

In Figure 17 the potential flow solution is illustrated for a blade with stagger angle of 60 degrees at the mean radius. An angle of attack of 7 degrees, corresponding approximately to design

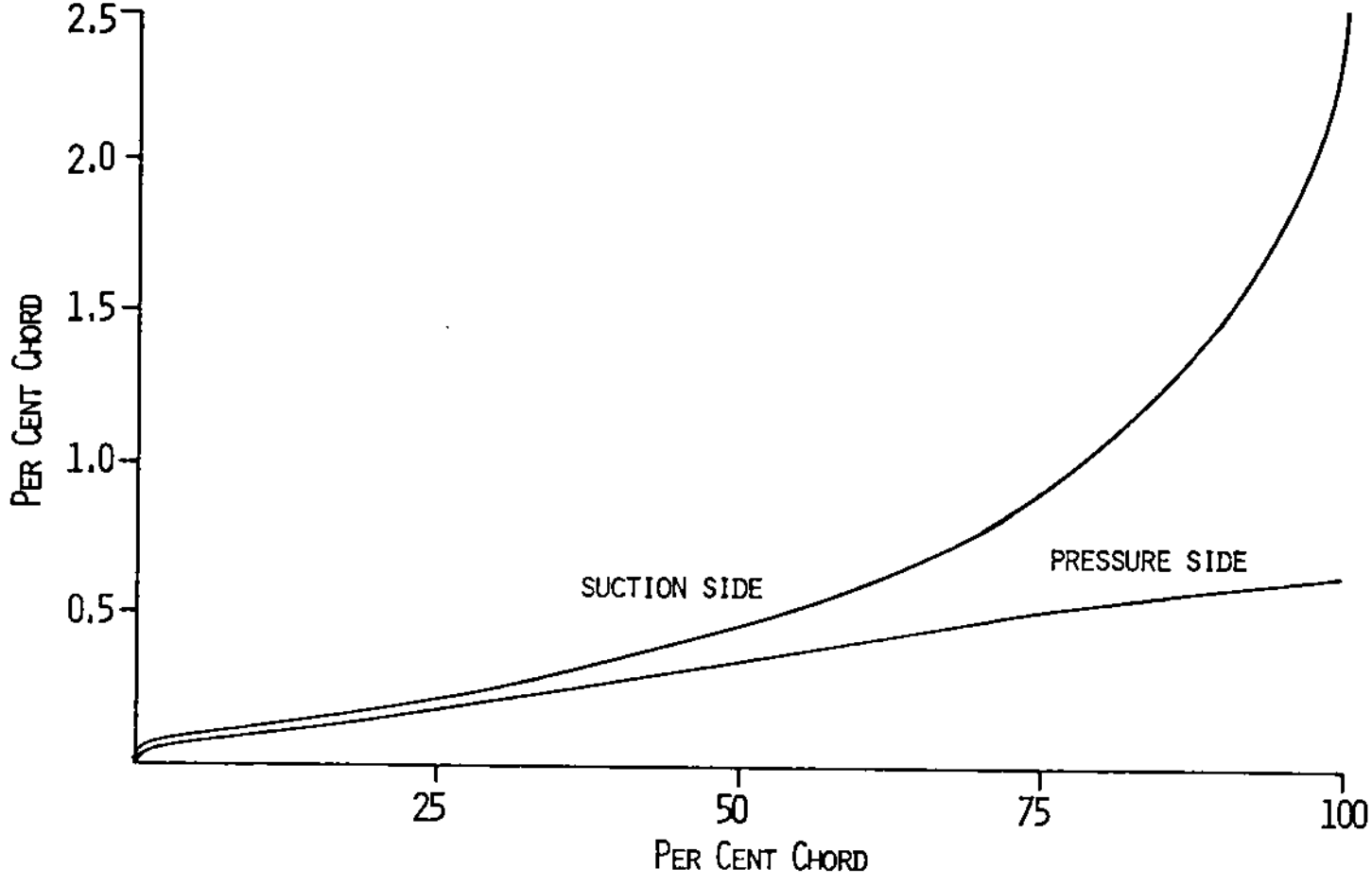

FIGURE 16. BOUNDARY LAYER THICKNESS

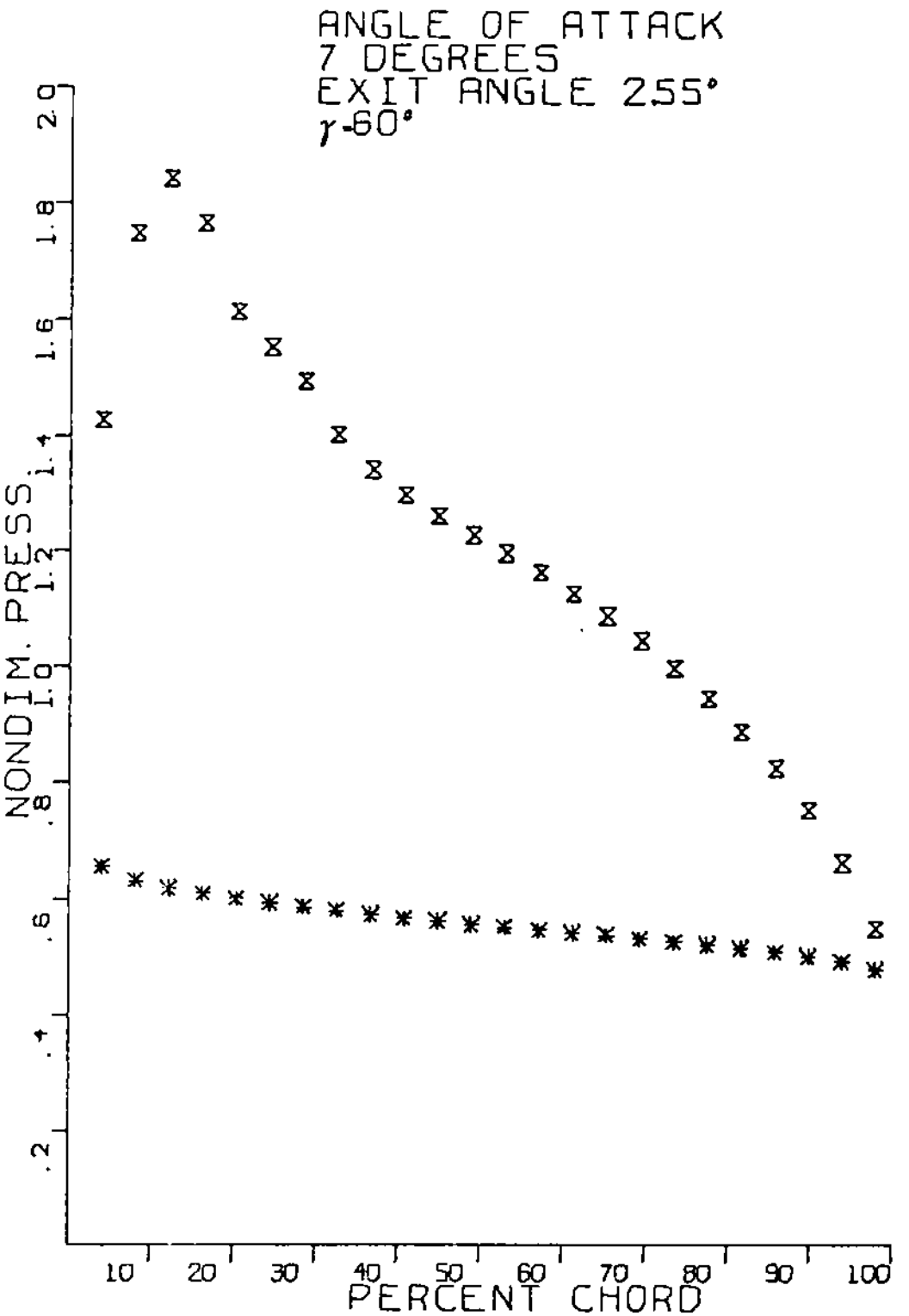

FIGURE 17. THEORETICAL PRESSURE DISTRIBUTION WITHOUT BL.

conditions for the compressor, was used. The Kutta condition was satisfied by trial and error to a turning angle of 9.55 degrees.

Figure 18 demonstrates the difference between the potential flow solution with and without boundary layer at the mean radius with a stagger angle of 60 degrees.

The theoretical solution at midspan, with boundary layers, for angles of attack of 5, 7, and 9 degrees is shown in Figure 19, a through c, and for 25 and 75 per cent span at an angle of attack of 7 degrees in Figure 20 a and b.

The turning angles were determined by trial and error until the trailing edge condition was satisfied. The trailing edge condition employed with the boundary layer solutions was the so-called closure hypothesis [16]. This trailing edge hypothesis was to set the turning angle so that the intersection of the pressures from the two surfaces occurs at the trailing edge, thus similar to the Kutta condition.

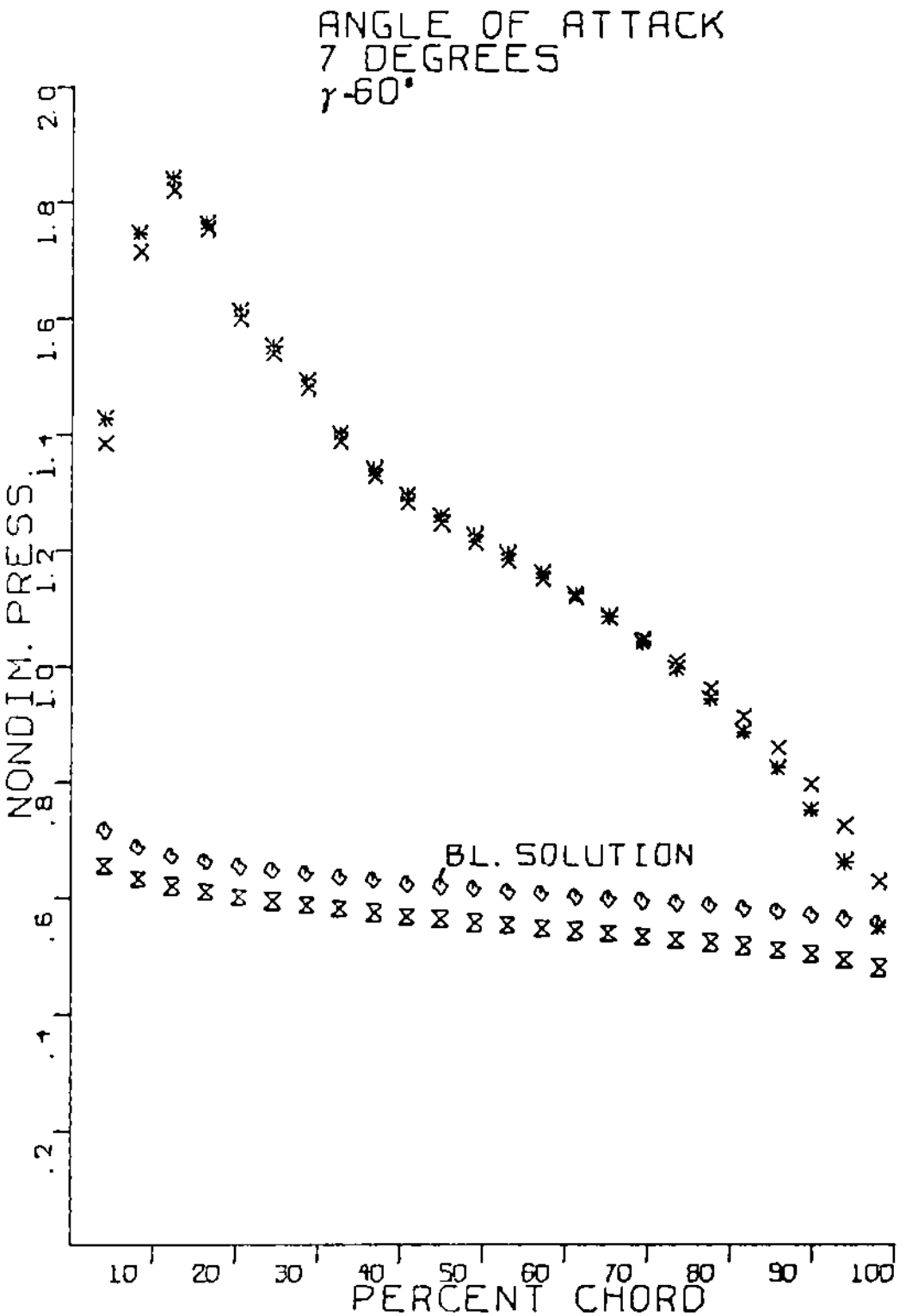

FIGURE 18. COMPARISON OF SOLUTION WITH AND WITHOUT BL.

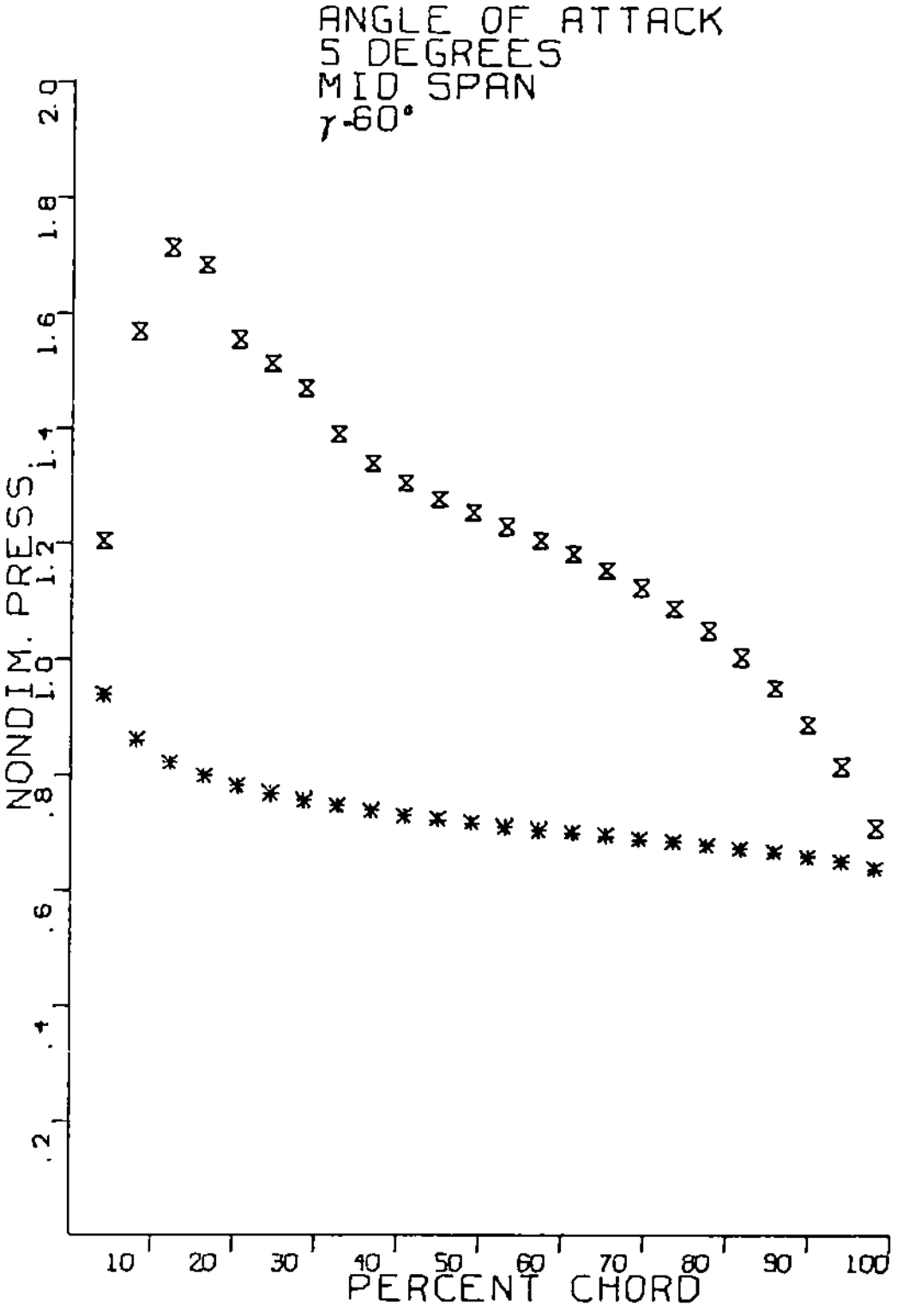

FIGURE 19a. THEORETICAL PRESSURE DISTRIBUTION WITH BL.

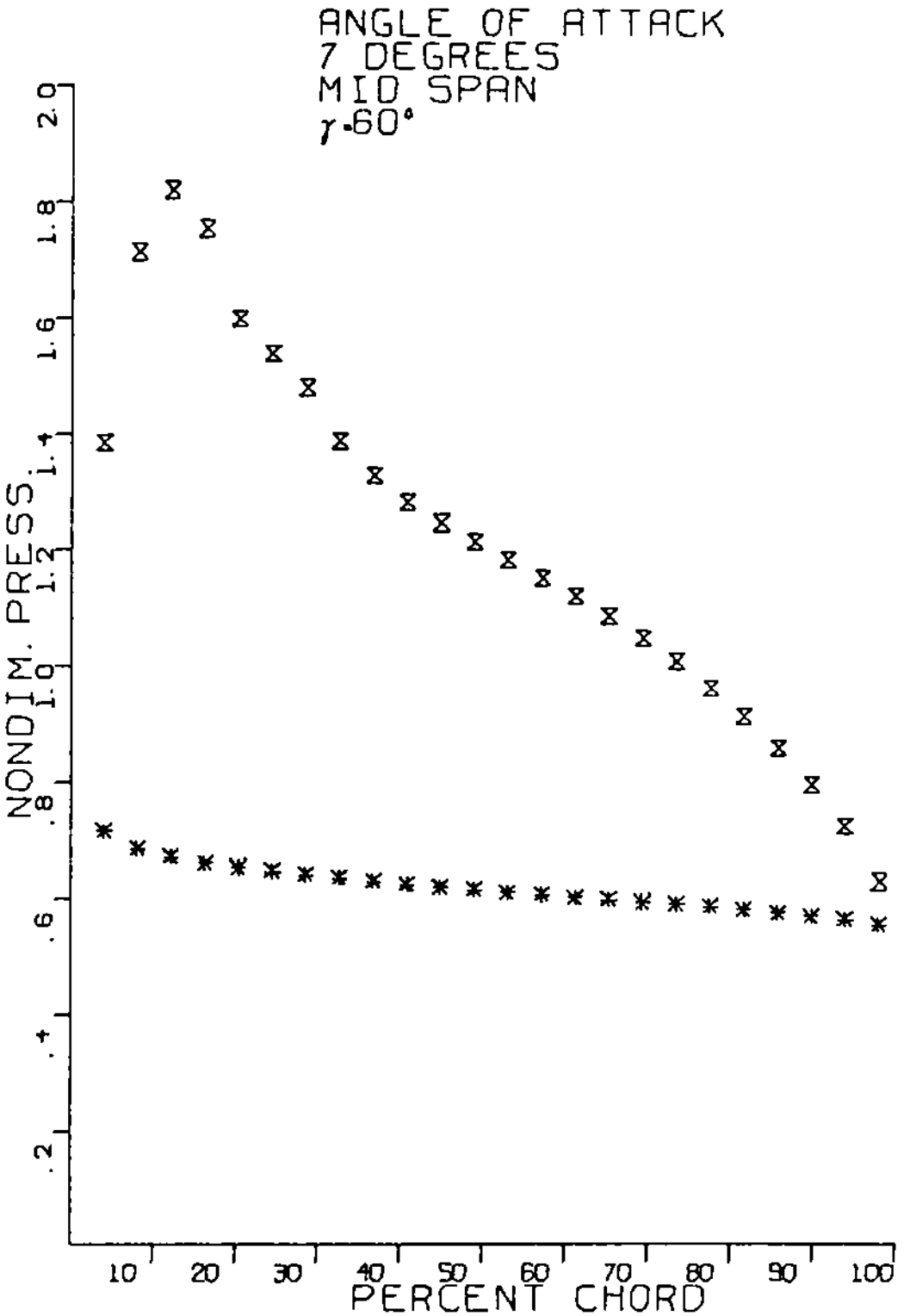

FIGURE 19b. THEORETICAL PRESSURE DISTRIBUTION WITH B.L.

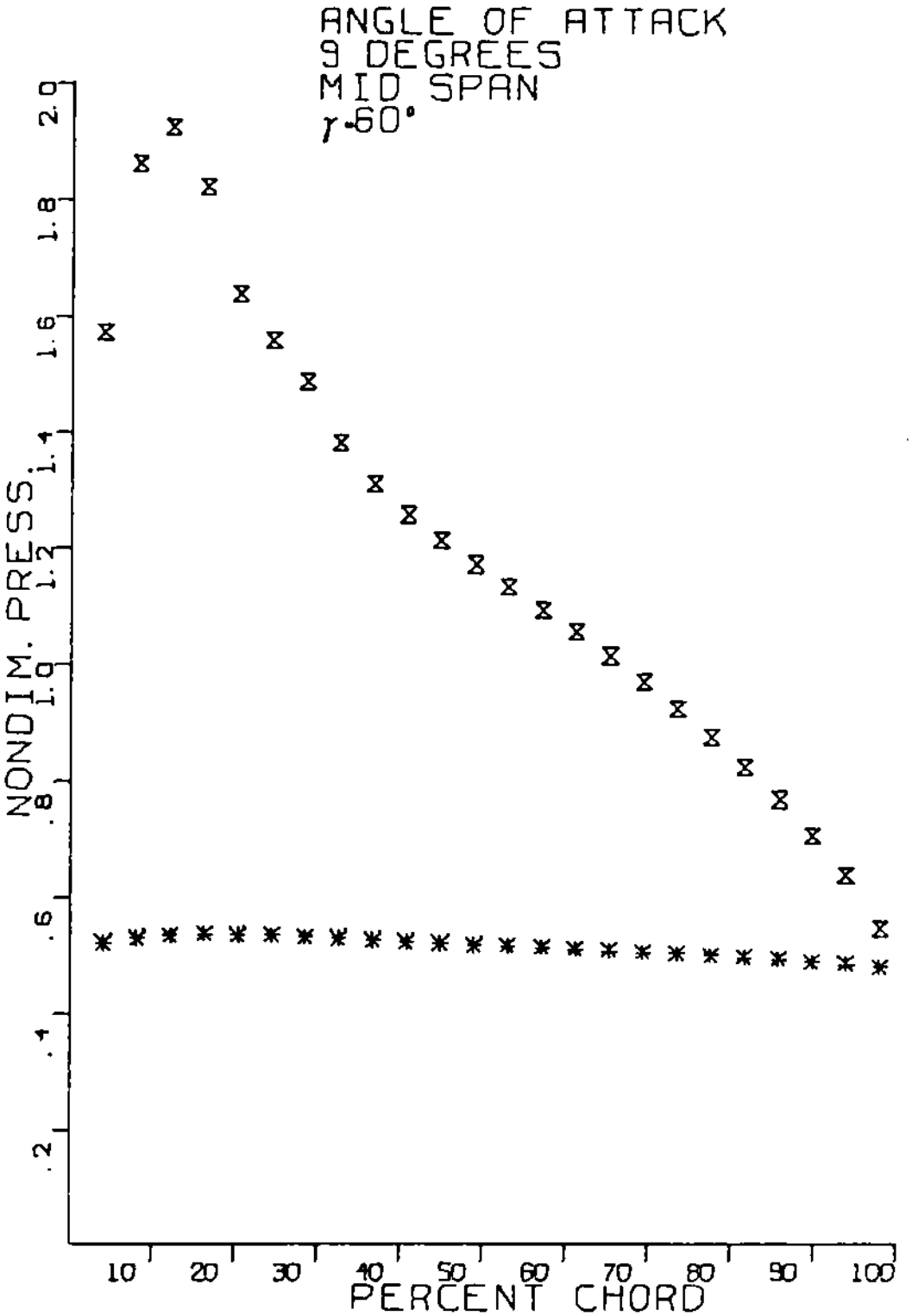

FIGURE 19c. THEORETICAL PRESSURE DISTRIBUTION WITH BL.

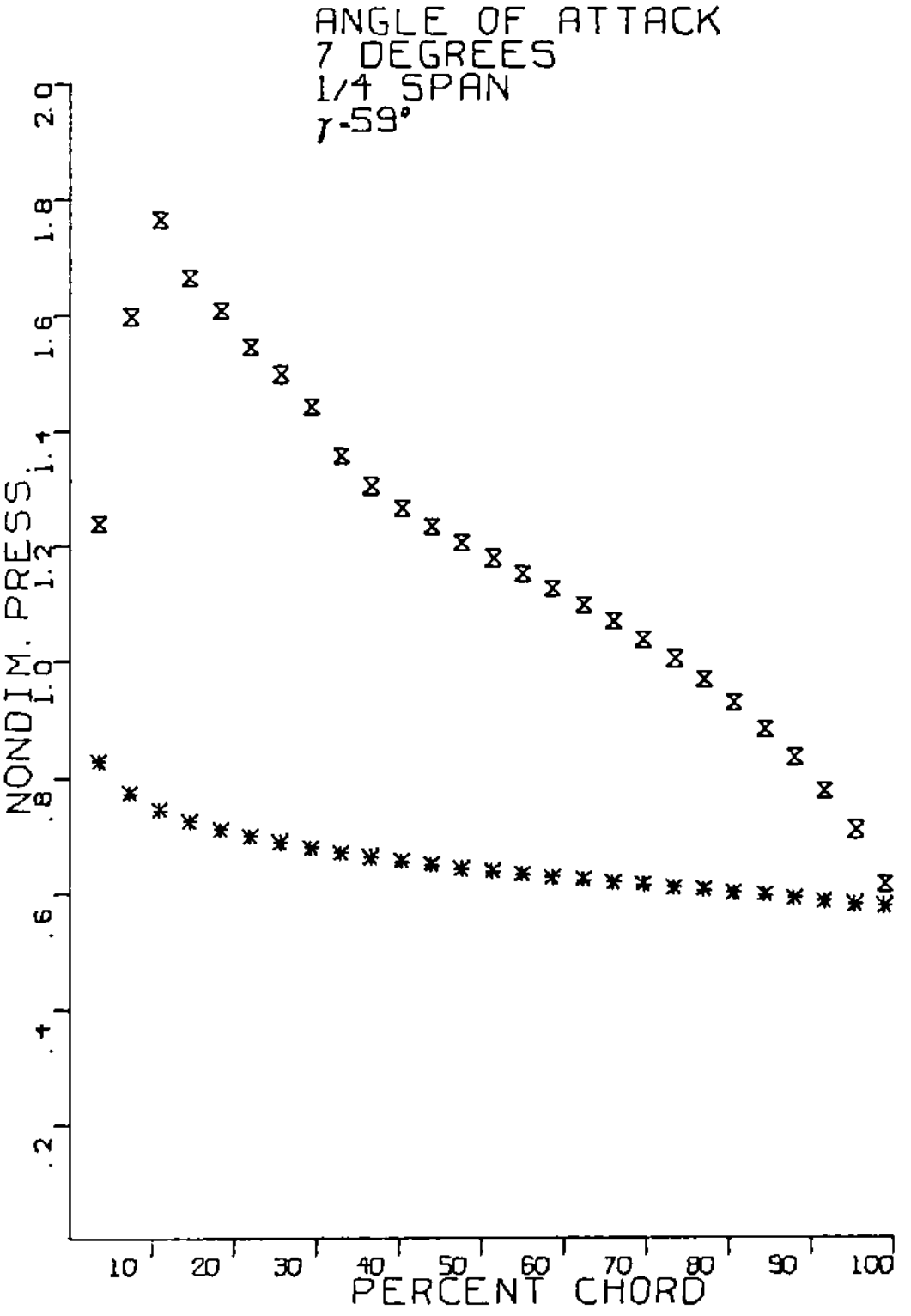

FIGURE 20a. THEORETICAL PRESSURE DISTRIBUTION WITH BL.

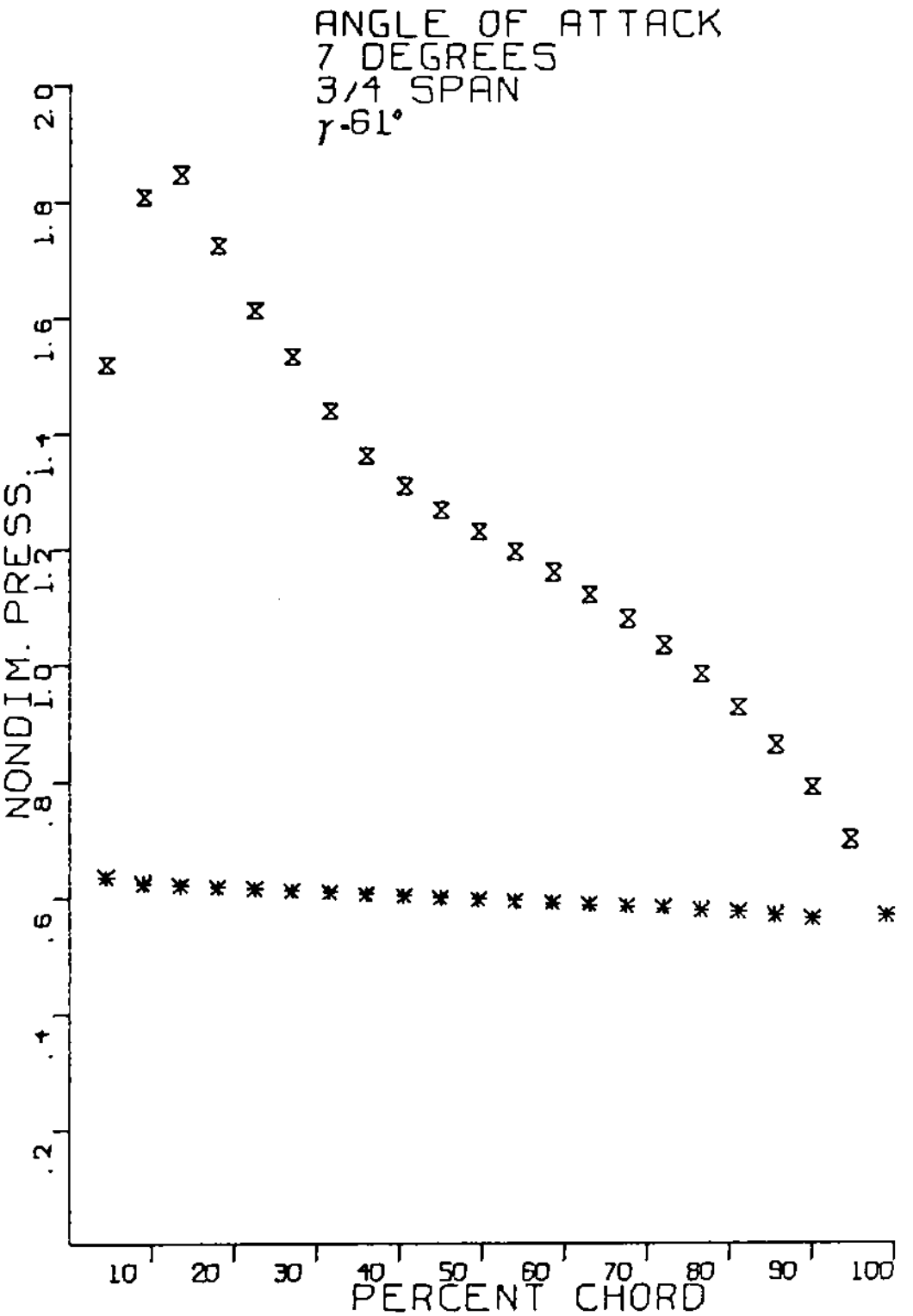

FIGURE 20b. THEORETICAL PRESSURE DISTRIBUTION WITH BL.

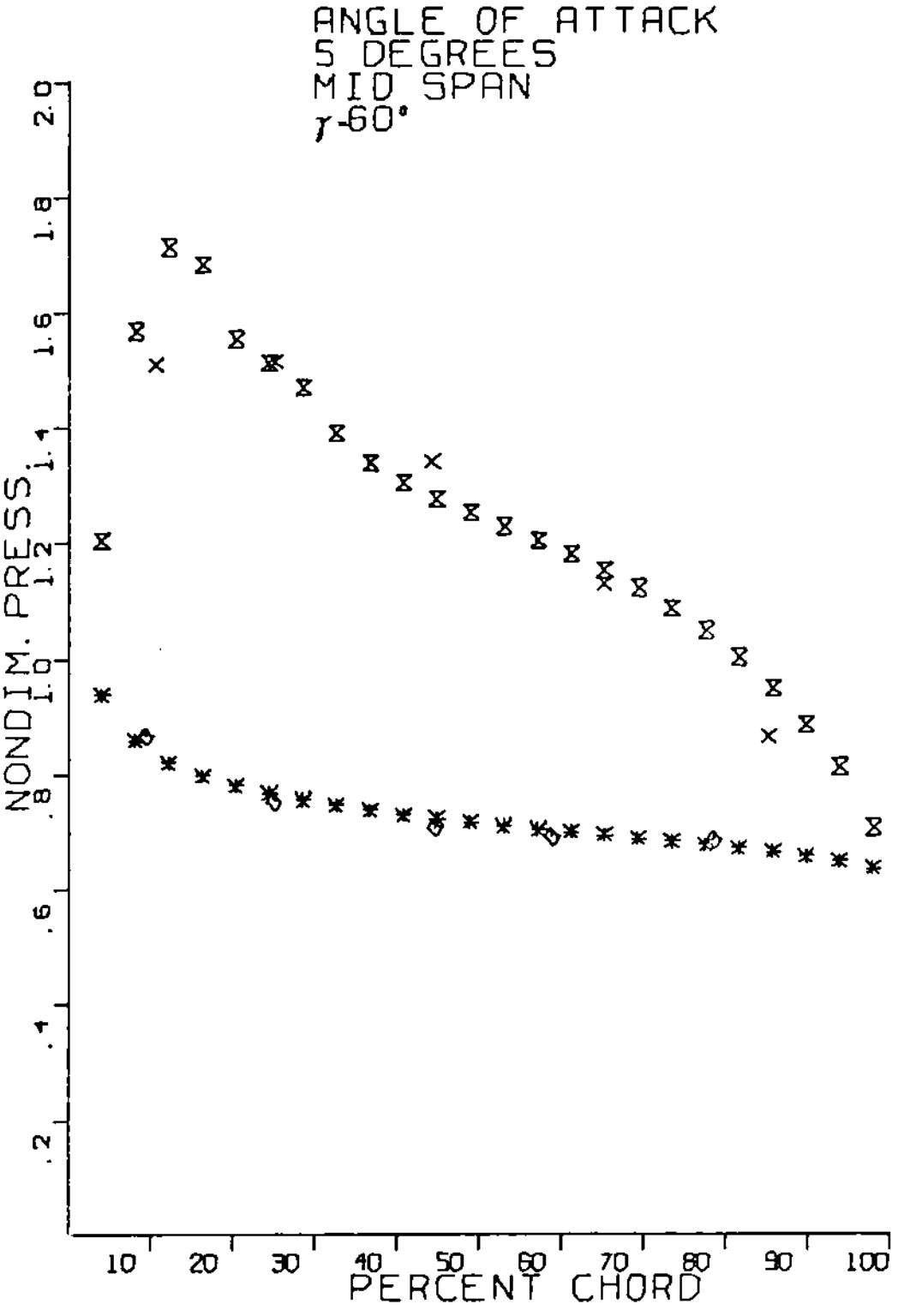

FIGURE 21a. COMPARISON OF EXP. AND THEOR. PRESSURE DIST.

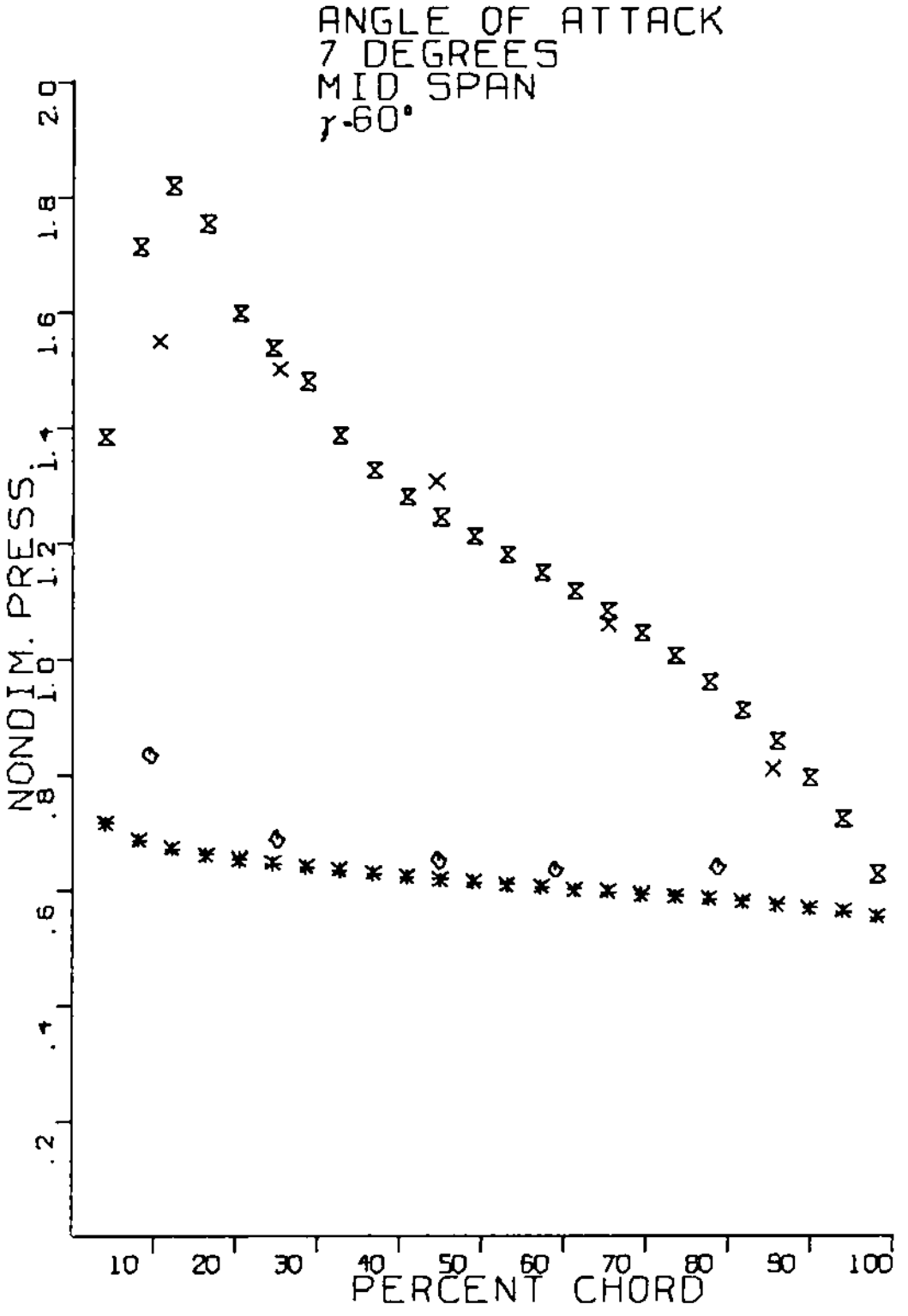

FIGURE 21b. COMPARISON OF EXP. AND THEOR. PRESSURE DIST.

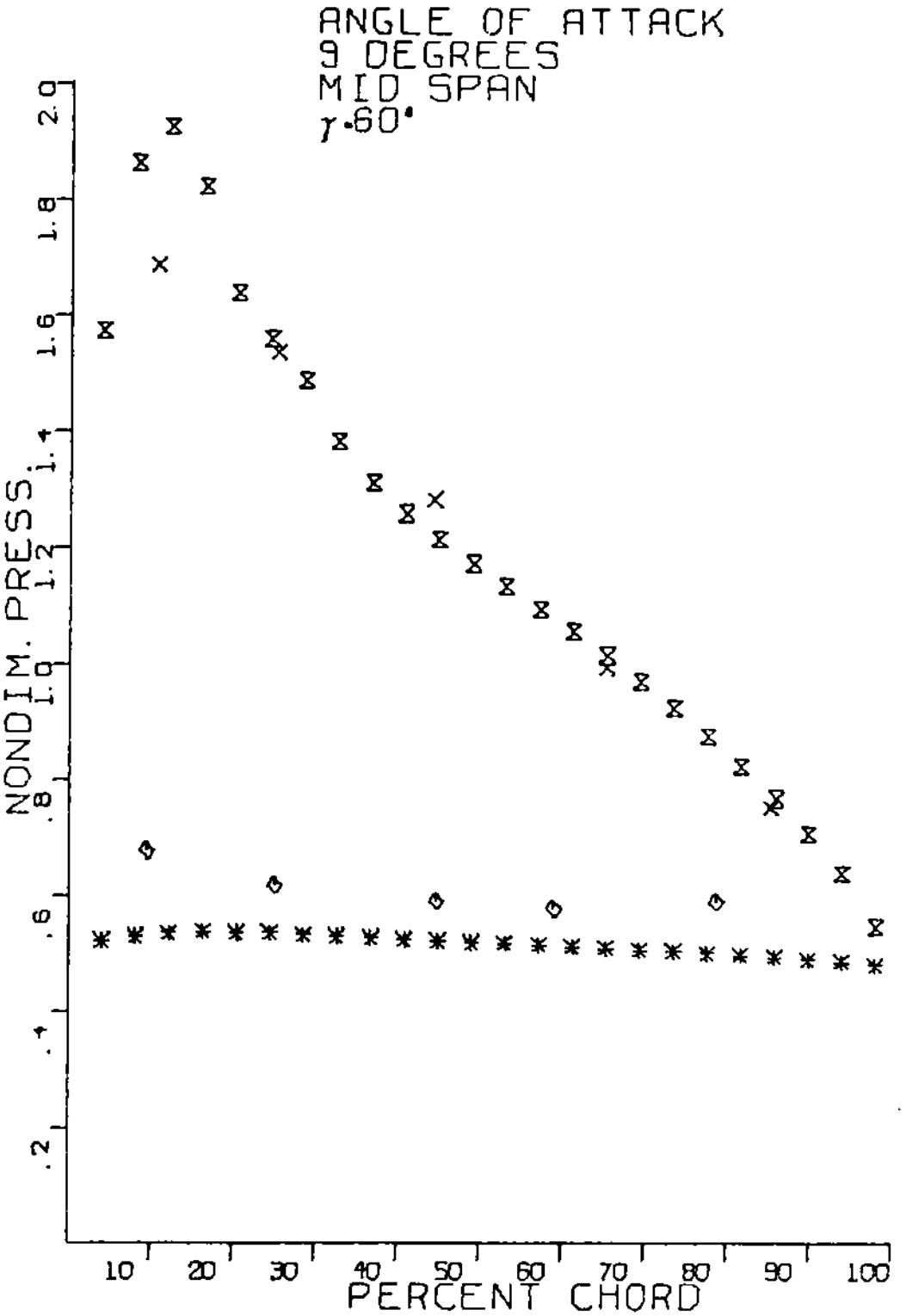

FIGURE 21c. COMPARISON OF EXP. AND THEOR. PRESSURE DIST.

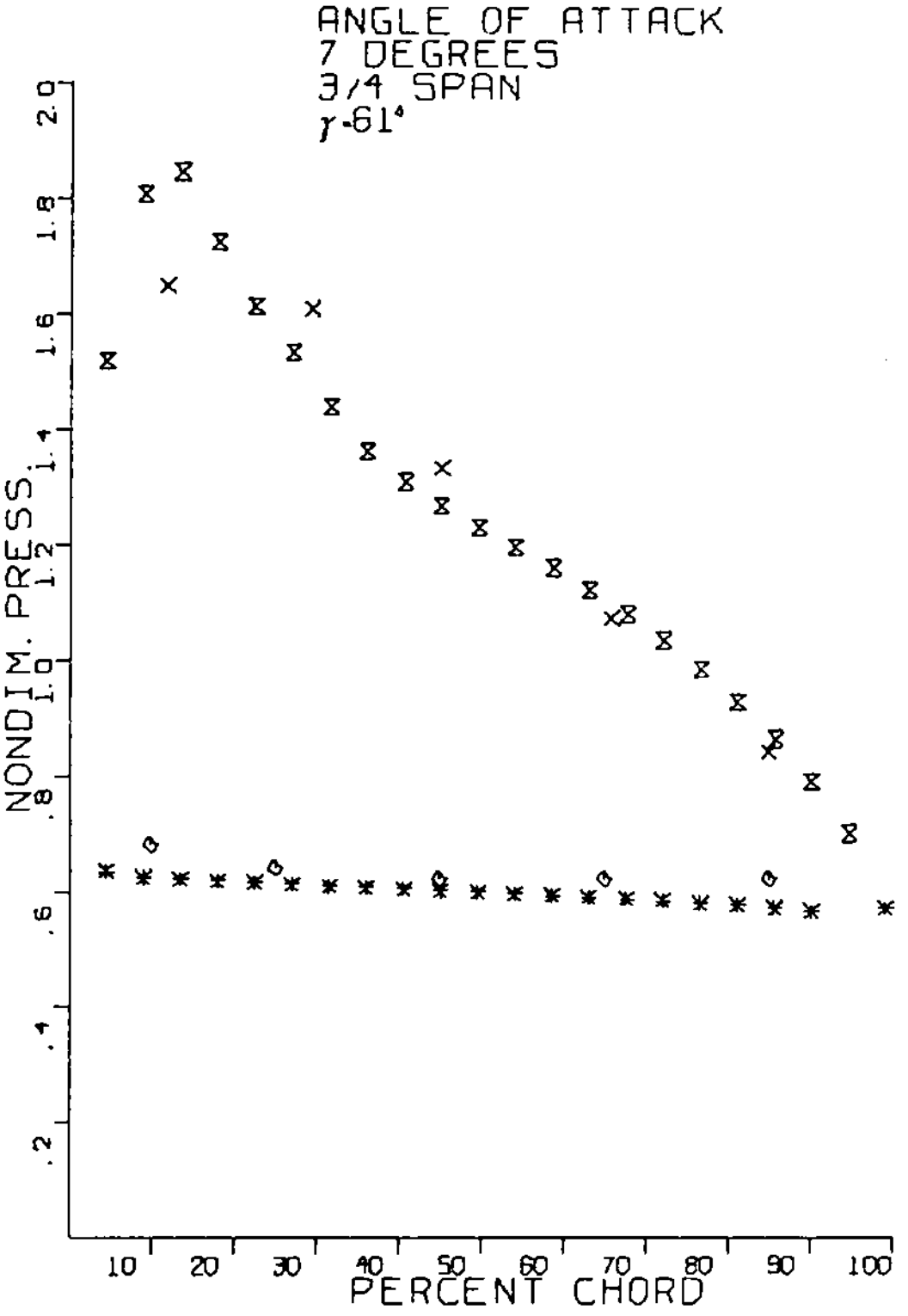

FIGURE 21d. COMPARISON OF EXP. AND THEOR. PRESSURE DIST.

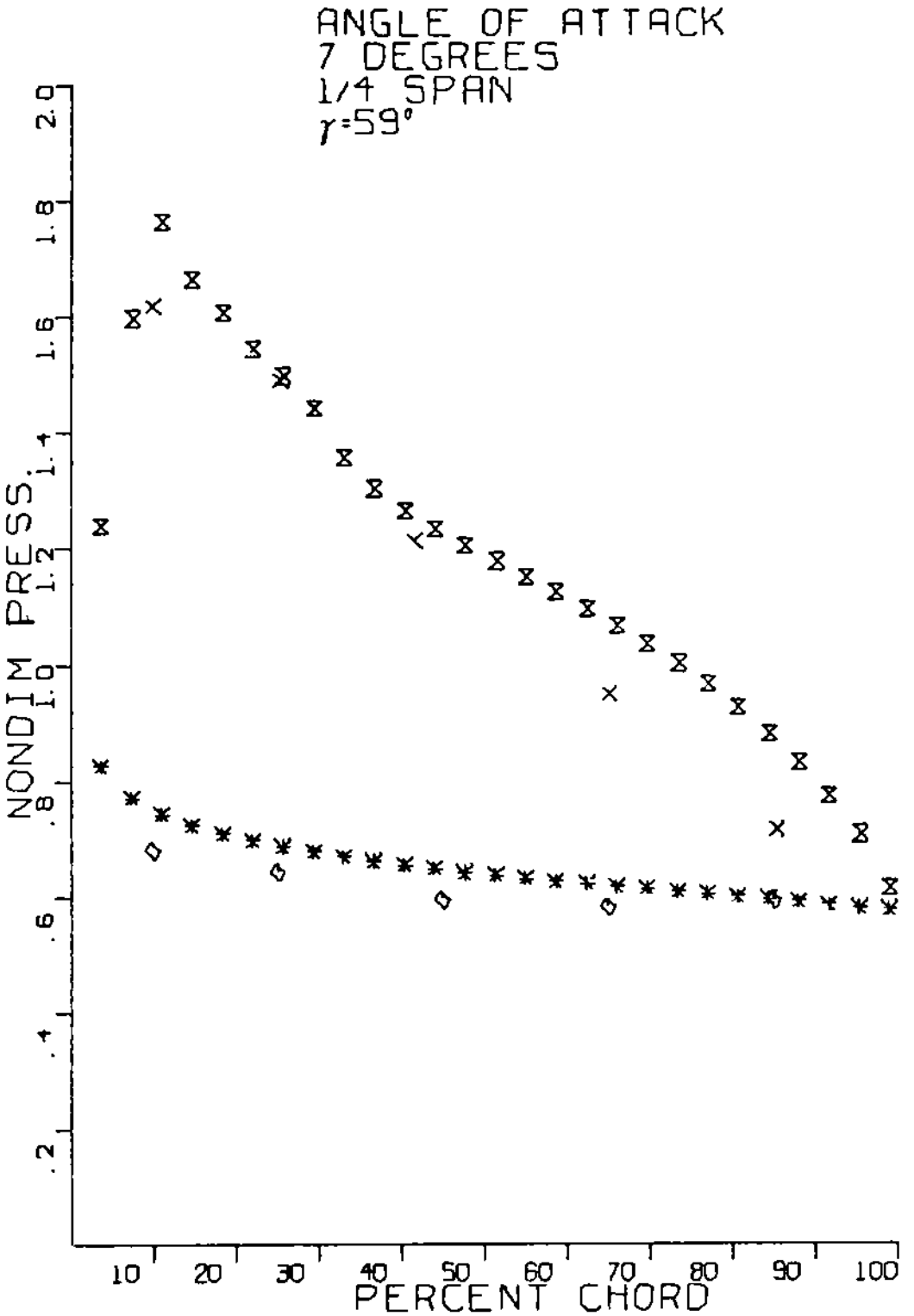

FIGURE 21e COMPARISON OF EXP. AND THEOR. PRESSURE DIST.

X. DISCUSSION OF RESULTS

Figure 12 a through j illustrates the experimental pressure distribution for various angles of attack and different span positions. The pressure distribution is consistent in figures a through e, with the highest pressure coefficient at 75% span and the lowest at 25% span, as expected. With increasing angle of attack, and accordingly lower absolute velocity, the pressure coefficient decreased.

The suction side pressure coefficient drops for 25% span at an angle of attack of 9 degrees and at about 45% chord, while for other span positions the distribution is consistent, Figure 12f. This is probably due to separation and reattachment since a pressure recovery occurs towards the trailing edge.

At higher angles of attack, in the stall region for the compressor, this pattern of separation and reattachment appeared for the other span positions also. In Figure 12i it is seen that the flow apparently separates at the leading edge for 75% and 50% span, and the separation occurs at about mid chord for 25% span. This was consistent with valve position 9 (Figure 12j).

A comparison between experimental and theoretical results is shown in Figure 21a through e. It is illustrated for midspan with an angle of attack of 5, 7 and 9 degrees. The agreement is good for 5 and 7 degrees, while the pressure side at 9 degrees angle of attack has a discrepancy of about 15%. This is probably due to the boundary layer at higher incident angles being thicker than the boundary layer used

in the program.

Figure 21 d and e shows the comparison of experimental and theoretical results for 25 and 75 per cent span at an angle of attack of 7 degrees. At 25 per cent span the difference is about 20%, probably due to the boundary layer used in the program being too thick. The agreement for 75 per cent span is good.

The peak at about 12% chord for the theoretical results did not appear for any angle of attack or span position for the experimental results. The reason for this was probably that in viscous flow a boundary layer develops so that the surface appears smoother and sharp peaks do not occur.

The accuracy of the experimental data for the blade surface pressures was high. The difference between the data obtained from different runs was a maximum of 0.2 inches of water at a magnitude of 10 inches of water. The comparison of stagnation pressures measured with a stationary probe showed good agreement (Table 2). The pressure transducer used had a linearity within ±0.06 per cent.

XI. CONCLUSIONS

Experiments have been carried out to obtain the pressure distribution on a rotating compressor blade at various angles of attack and span positions. These distributions followed in general a consistent pattern, however, slightly different from previous work [10]. Employing a potential flow solution with boundary layers seems justified from the comparison between theoretical and experimental results. A more accurate displacement thickness could perhaps achieve a better agreement in some cases. In other cases the results show surprisingly good coherence. The boundary layer used in the program was thin, which also justifies the prediction of boundary layers from potential flow velocities. The boundary layer was thin since the flow was assumed to be unseparated all along the blade surface.

XII. RECOMMENDATIONS

This investigation showed that there are several connected areas which suggest further study.

The following are considered to be especially pertinent.

1. Investigate the radial distribution of the boundary layer on the compressor blade.
2. Develop an improved method for determining the theoretical deviation angle.
3. Further study in the fluctuating pressure area.

XIII. REFERENCES

1. Weske, J. R., "An Investigation of the Aerodynamic Characteristics of a Rotating Axial-Flow Blade Grid," NACA Tech. Note No. 1128, 1947.

2. Weske, J. R., "Fluid Dynamic Aspects of Axial-Flow Compressors and Turbines," Journal of the Aeronautical Sciences, Vol. 14, November 1947, pg. 651-656.

3. Runckel, R. F. and Davey, R. S., "Pressure Distribution Measurements on the Rotating Blades on a Single Stage Axial-Flow Compressor," NACA Tech. Note No. 1189, 1947.

4. Wu, C. H. and Wolfenstein, L., "Application of Radial-Equilibrium Condition to Axial-Flow Compressor and Turbine Design," Rep. 955 NACA, 1950.

5. Westphal, W. R. and Godwin, W. R., Comparison of NACA 65-Series Compressor Blade Pressure Distributions and Performance in a Rotor and in a Cascade," NACA Tech. Note No. 3806, 1951.

6. Schlichting, H., "Problems and Results of Investigations on Cascade Flow," Journal of the Aeronautical Sciences, Vol. 21, March 1954, pg. 163-178.

7. Johnsen, I. A. and Bullock, R. O., Aerodynamic Design of Axial-Flow Compressors, SP-36 NASA, 1965.

8. Weyer, H. and Schodl, R., "Development and Testing of Techniques for Oscillating Pressure Measurements Especially Suitable for Experimental Work in Turbomachinery," ASME, No. 71-FE-28.

9. Sexton, M. R., Instrumentation for Pressure Measurements on a Rotating Blade in an Axial-Flow Compressor, M.S. Thesis, VPI&SU, 1972.

10. Warren, J. W., A Theoretical Approach for Obtaining Pressure Distributions on the Rotor of an Axial-Flow Compressor Using Radial Equilibrium and a Blade to Blade Computer Program, M.S. Thesis, VPI&SU, 1973.

11. Bryner, H., Potential Flow Solution and Incompressible Boundary Layer for a Two-Dimensional Cascade, M.S. Thesis, VPI&SU, 1974.

12. White, F. M. "Viscous Fluid Flow," McGraw-Hill, 1974.

13. Cohen, H. and Rogers, G. F. C. and Saravanamuttoo, H. I. H., "Gas Turbine Theory," Longman, 1974.

14. Currie, I. G., Fundamental Mechanics of Fluids, McGraw-Hill, 1974.

15. Miller, M. J. and Serovy, G. K., Deviation Angle Estimation Using Inviscid Flow Solutions, ASME 74-GT-74.

APPENDIX A

The frequency response for a pipe and a cavity may be calculated with Helmholtz resonator frequency theory, taken from reference 13.

$$w = \frac{\pi r^2 c^2}{V[L + \frac{1}{2}\sqrt{\pi^2 r^2}]}^{\frac{1}{2}}$$

$c = \sqrt{kRT}$ the velocity of sound

$k = 1.4$

$R = 0.287 - 10^3$ J/K

$T = 298$ K

$\therefore$ C = 346 m/S

V is the volume in the connection to the pressure transducer.

L is the length of the tubing from the rotor blade to the transducer.

r is the inside diameter.

$V = 819 \cdot 10^{-9}$ m

$L = 0.178 + 0.203 = 0.381$ m

$r = 0.00041$ m

$$w = \frac{\pi \cdot 0.00041^2 \cdot 346^2}{8.19 \cdot 10^{-9}(0.381 + \frac{1}{2}\sqrt{\pi^2}\ 0.00041^2)}^{\frac{1}{2}} = 4497 \text{ rad/S}$$

which yields a resonant frequency of 716 Hz.

Since the volume of the cavity in the transducer was so small, it is doubtful if Helmholtz resonator frequency was applicable. The

resonate frequency may instead be calculated by using organ pipe assumptions.

The minimum time required for a pulse to be reflected back to the starting point was

$$t = \frac{2 \cdot 0.381}{346} = 2.2 \cdot 10^{-3} \text{ S}$$

which gives a frequency of 454 Hz.

APPENDIX B

Table 3. Pressures and Angles Measured With Stationary Probe

valve position	P_1 inches of water	(kPa)	P_{o1}	α_1	P_2 inches of water	(kPa)	P_{o2} inches of water	(kPa)	α_2
0	-2.20	(-0.547)	0	23	0.72	(0.179)	2.35	(0.585)	-4
1	-2.00	(-0.498)	0	23	0.95	(0.236)	2.55	(0.635)	-7
2	-1.90	(-0.473)	0	23	1.17	(0.291)	2.77	(0.689)	-9
3	-1.80	(-0.448)	0	23	1.45	(0.361)	2.95	(0.734)	-12
4	-1.60	(-0.398)	0	23	1.70	(0.423)	3.08	(0.766)	-16
5	-1.30	(-0.323)	0	23	1.90	(0.473)	3.17	(0.789)	-22
6	-1.00	(-0.249)	0	22	1.90	(0.473)	3.15	(0.784)	-32
7	-0.85	(-0.212)	0	22	1.90	(0.473)	2.95	(0.734)	-37
8	-0.80	(-0.199)	0	22	1.87	(0.465)	2.70	(0.672)	-37
9	-0.75	(-0.187)	0	22	1.87	(0.465)	2.70	(0.672)	-38

Table 4. Velocities at Mean Radius

valve position	C_1 m/s	α_1 (Degrees)	C_a m/s	C_{w1} m/s	V_1 m/s	β_1 (Degrees)
0	31.64	23	29.11	12.37	67.36	68.4
1	30.18	23	27.77	11.80	66.85	65.7
2	29.41	23	27.07	11.49	65.78	66.2
3	28.62	23	26.33	11.19	65.26	67.2
4	26.97	23	24.84	10.55	64.10	68.9
5	24.32	23	22.40	9.51	62.24	70.7
6	21.34	22	19.78	7.99	59.86	71.9
7	19.66	22	18.23	7.38	58.67	71.9
8	19.08	22	17.68	7.16	61.87	73.4
9	18.47	22	17.13	6.92	57.94	72.8

Table 5. Velocities at 25 Per Cent Span
Obtained by Radial Equilibrium

valve position	C_1 m/s	α_1 (Degrees)	C_a m/s	C_{w1} m/s	V_1 m/s	β_1 (Degrees)
0	32.11	25	29.11	13.64	64.50	63.2
1	30.66	25	27.77	13.00	63.40	64.0
2	29.88	25	27.07	12.66	62.39	64.5
3	29.08	25	26.33	12.33	62.21	65.0
4	27.43	25	24.84	11.62	60.90	65.9
5	24.73	25	22.40	10.48	58.89	67.6
6	21.65	25	19.78	8.80	56.39	69.5
7	19.96	24	18.23	8.13	55.20	70.7
8	18.76	24	17.68	7.89	54.80	71.2
9	18.75	24	17.13	7.63	54.38	71.6

Table 6. Velocities at 75 Per Cent Span
Obtained by Radial Equilibrium

valve position	C_1 m/s	α_1 (Degrees)	C_a m/s	C_{w1} m/s	V_1 m/s	β_1 (Degrees)
0	31.24	21	29.11	11.34	70.56	65.6
1	29.69	21	27.77	10.79	69.56	66.5
2	29.05	21	27.07	10.52	69.01	66.9
3	28.25	21	26.33	10.24	68.46	67.4
4	26.64	21	24.84	9.66	67.36	68.4
5	28.05	21	22.40	8.72	65.59	70.0
6	21.09	20	19.78	7.59	63.43	71.8
7	19.45	20	17.98	6.77	62.45	73.0
8	18.84	20	17.68	6.55	62.09	73.5
9	18.26	20	17.13	6.34	61.72	73.9

APPENDIX C

Boundary Layer for the Pressure Side

To obtain a boundary layer thickness on the pressure side a flat plate assumption was employed, and the flow was assumed to be turbulent.

The starting equation was the momentum integral equation, derived by Von Kármán in 1921, as shown in reference 13.

$$\frac{d\theta}{dx} + (2 + H)\frac{\theta}{U_e}\frac{dU_e}{dx} = \frac{C_f}{2} \qquad (1)$$

where $\theta = \int_0^\infty \frac{\bar{u}}{U_e}\left(1 - \frac{\bar{u}}{U_e}\right) dy$ momentum thickness

$H = \frac{\delta^*}{\theta}$ momentum shape factor

$H = 1.38$ for a flat plate

$\delta^* = \int_0^\infty \left(1 - \frac{\bar{u}}{U_e}\right) dy$ displacement thickness.

The boundary conditions used were;

$\bar{u}(x,y) = 0 \quad \bar{v}(x,y) = 0$ no slip condition on the surface.

$\bar{u}(x,\delta) = U_e(x)$ the velocity outside the boundary layer equal to the freestream velocity.

The variable of interest was the displacement thickness δ^*, and the goal was to achieve a numerical value for δ^* as a function of the chord length x.

For a flat plate the pressure gradient was assumed to be zero, and equation 1 reduces to 2.

$$C_f = 2 \frac{d\theta}{dx} \tag{2}$$

The Reynold's number with the parameter θ and the parameter x was respectively,

$$Re_\theta = \frac{U_e \theta}{\nu} , \quad Re_x = \frac{U_e x}{\nu}$$

introduced in equation 2 yields

$$C_f = 2 \frac{d\ Re_\theta}{d\ Re_x}$$

Since the pressure gradient was assumed to be zero, C_f was a function of only one arbitrary parameter, ex. $C_f = C_f(Re_\theta)$. Hence

$$Re_x = 2 \int_o^{Re_\theta} \frac{d\ Re_\theta}{C_f(Re_\theta)} \tag{3}$$

To obtain a relation for $C_f(Re_\theta)$, the law of the wall and wake relations were used.

$$\frac{\theta}{\delta} = \frac{1 + \Pi}{k\lambda} - \frac{2 + 3.179\ \Pi + 1.5\ \Pi^2}{k^2\ \lambda^2} \tag{4}$$

$$\lambda = \frac{1}{k} \ln \frac{Re_\delta}{\lambda} + B - \frac{2}{k} \tag{5}$$

$$\lambda = \sqrt{\frac{2}{C_f}} \tag{6}$$

For a flat plate, $\Pi = 0.5$, $k = 0.4$ and $B = 5.5$. Equations 4, 5 and 6 can be approximated for the required relation for $C_f(Re_\theta)$

$$Re_\theta = \left(3.75 - \frac{24.778}{\sqrt{\frac{2}{C_f}}}\right) e^{0.4\left(\sqrt{\frac{2}{C_f}} - 8\right)}$$

This is fitted to a more convenient power law approximation, and the relation $H = 1.38$ for a flat plate yields

$$C_f = 0.0128\ Re_{\delta^*}^{-1/6} \tag{7}$$

with an accuracy within ±4 per cent.

Equation 7 was used in equation 3 to accomplish a relation between Re_{δ^*} and Re_x.

$$Re_{\delta^*} = 0.018\ Re_x^{6/7} \tag{8}$$

From equation 8 the displacement thickness as a function of the chord length was obtained.

$$\delta^* = 0.018 \left(\frac{\nu}{u}\right)^{1/7 \times 6/7} \tag{9}$$

Equation 9 was the desired relation between δ^* and x.

Appendix D
Computer Program

```
      DIMENSION SF(200,40),YL(200),YU(200),DYL(200),XF(10),XB(10)
      DIMENSION VL(200),VU(200)
      DIMENSION VEL(50)
      DIMENSION INF(10),INF1(10) ,XI(54),YI(54)
      DATA INF/'   P','ERCE','NT C','HORD','    ','    ','    ','    ',
     $'    ','    '/
      DATA INF1/'  NO','NDIM','. PR','ESS.','    ','    ','    ','    ',
     $'    ','    '/
C
C     GRID GEOMETRY AND INPUT
C
C     ANGLE OF ATTACK 7  DEGREES
C
      PI=3.1415926
      B1=7.00*PI/180
      B2=2.40*PI/180.
      GAM=59.*PI/180.
      IGAM=ABS(GAM*180./PI-59.)+0.0001
      IF(IGAM.EQ.0.) SCALE=24./(2.*PI*6.89063*COS(GAM))
      IF(IGAM.EQ.1.) SCALE=24./(2.*PI*7.59375*COS(GAM))
      IF(IGAM.EQ.2.) SCALE=24./(2.*PI*8.29688*COS(GAM))
      V1=1./((1.-TAN(B1)*TAN(GAM))*COS(B1))
      V2=V1*COS(GAM+B1)/COS(GAM-B2)
      N1=25
      N2=40
      N4=100
      M=12
      DX=TAN(GAM)/25.
      DY=1.0/12.
      YBS=0.01
      BC=1.687*SCALE
      N3=BC/DX+40
```

```
      N12=N1+N2
      N13=N1+N3
      N14=N1+N4
C
C     BOUNDARIES AND BLADE GEOMETRY
C
      C1=1.382421
      D1=-7.314691
      E1=28.40476
      C2=0.202583
      D2=0.225093
      NZ=N14+1
      DO 60 I=1,NZ
      YL(I)=-DY/2.
      DYL(I)=0.0
   60 YU(I)=1.0+1.5*DY
      YL(N2+1)=0.001
      X=0.
      NZ=N2+2
      NZ1=N3+1
      DO 61 I=NZ,NZ1
      X=X+DX/BC
      BLS=0.027*X-0.067*X**2+0.081*X**3
      DBLS=(0.027-2*0.067*X+3*X*0.081*X**2)*1.678
      IF(X-0.3)   62,63,63
   62 X1=0.3-X
      Y1=C1*X1**2+D1*X1**3+E1*X1**4
      DY1=2.*C1*X1+3.*D1*X1**2 +4.*E1*X1**3
      YL(I)=(0.187-YBS-Y1+BLS)*SCALE
      DYL(I)=(DY1+DBLS)/1.687
      GO TO 611
   63 X2=X-0.3
```

```
      Y2=C2*X2**2+D2*X2**3
      DY2=2.*C2*X2+3.*D2*X2**2
      YL(I)=(0.187-YBS-Y2+BLS)*SCALE
      DYL(I)=(-DY2+DBLS)/1.687
  611 CONTINUE
      WRITE(6,115)    X,YL(I),DYL(I)
  115 FORMAT(3F10.5)
   61 CONTINUE
      YU(N12+1)=0.9999
      NZ=N12+2
      NZ1=N13+1
      X=0.0
      DO 64 I=NZ,NZ1
      X=X+DX
      BLP=0.008*X
   64 YU(I)=1.0-(YBS+BLP)*SCALE
      Y=0.
      DO 65 J=2,5
      XB(J)=0.0
      XF(J)=0.0
      Y=Y+DY
      Y11=0.187-YBS-Y/SCALE
      IF(Y11)65,65,509
  509 X1=0
      Y1=0.
   66 X1=X1+0.001
      Y1P=Y1
      X=0.3-X1
      Y1=C1*X1**2+D1*X1**3+E1*X1**4
      BLS=0.027*X-0.067*X**2+0.081*X**3
      Y1=Y1-BLS
      IF(Y11-Y1)    67,67,66
```

```
   67 X1=X1-.001*(Y1-Y11)/(Y1-Y1P)
      XF(J)=(0.3-X1)*BC
      X2=0
      Y2=0
   68 X2=X2+0.002
      X=X2+0.3
      IF (X-2.1) 681,65,65
  681 CONTINUE
      BLS=0.027*X-0.067*X**2+0.081*X**3
      Y2P=Y2
      Y2=C2*X2**2+D2*X2**3
      Y2=Y2-BLS
      IF(Y11-Y2)   69,69,68
   69 X2=X2-.002*(Y2-Y11)/(Y2-Y2P)
      XB(J)=(0.3+X2)*BC
   65 CONTINUE
      WRITE(6,101)   SCALE,V2,DX,DY,BC
  101 FORMAT(5F10.6)
      X=0.
      NZ=N14+1
      DO 110 I=1,NZ
      X=X+DX
      WRITE(6,102)   I,X,YU(I),YL(I)
  102 FORMAT(I4,3F10.5)
  110 CONTINUE
      DO 107 J=2,5
      WRITE (6,108)  XF(J),XB(J)
  108 FORMAT(2F10.6)
  107 CONTINUE
C
C     INITIAL VALUES
C
```

```
      NZ=N1+N4+1
      DO 10 I=1,NZ
      DO 11 J=1,5
   11 SF(I,J)=0.0
      MZ=M+2
      DO 12 J=6,MZ
   12 SF(I,J)=1.0
   10 CONTINUE
C
C
C     ITERATION LOOP
C
      DO 13 IT=1,2
      DO 14 ITT=1,1000
C
C     BOUNDARY VALUES
C
      DELS=0.048
      DO 71 I=1,N2
   71 SF(I,1)=SF(I+N1,M+1)-1.0
      MZ=M+2
      DO 72 J=2,MZ
   72 SF(1,J)=SF(1,1)+(J-1)*DY/(1.0-TAN(GAM)*TAN(B1))
      NZ=N1+1
      DO 73 I=2,NZ
   73 SF(I,M+2)=SF(1,M+2)-(I-1)*DX*TAN(B1)/(1.0-TAN(GAM)*TAN(B1))
      NZ=N3+2
      DO 74 I=NZ,N4
   74 SF(I,1)=SF(I+N1,M+1)-(1.0+DELS)
      MZ=M+1
      DO 75 J=1,MZ
   75 SF(N14+1,J)=SF(N14+1,M+2)-(M+2-J)*DY*(1.+DELS)/(1.+TAN(GAM)*TAN(B2
```

```
     $))
      NZ=N4+1
      DO 76 I=NZ,N14
   76 SF(I,1)=SF(N14+1,1)-(N14+1-I)*DX*TAN(B2)*(1.+DELS)/
     $(1.+TAN(GAM)*TAN(B2))
C
C     STREAM FUNCTION CALCULATION
C
      CHM=0.0
      DO 99 I=2,N14
      X=(I-N2-1)*DX
      MZ=M+1
      DO 98 J=2,MZ
      Y=(J-1)*DY
      DX1=DX
      DX2=DX
      DY1=DY
      DY2=DY
      SX1=SF(I-1,J)
      SX2=SF(I+1,J)
      SY1=SF(I,J-1)
      SY2=SF(I,J+1)
      IF (I-N2) 96,96,185
  185 CONTINUE
      NZ=N13+2
      IF (I-NZ) 189,182,96
  182 KZ=M+1
      IF (J-KZ)96,183,96
  183 NX=N13+1
      NX1=N3+1
      YZ2=YL(NX1)
      YZ1=1.0-YU(NX)
```

```
      SX1=1.0+YZ1/(YZ1+YZ2)*DELS
      IF(DELS.EQ.0.0) DX1=(N3-N2+1)*DX-EC
      GO TO 96
  189 CONTINUE
  181 CONTINUE
      IF(Y-YL(I))98,98,81
   81 CONTINUE
      IF(Y-YL(I))82,98,98
   82 CONTINUE
      Z=Y-DY
      IF(Z-YL(I))83,84,84
   83 CONTINUE
      DY1=Y-YL(I)
      SY1=0.0
      IF(Y-YL(I+1))87,86,86
   86 CONTINUE
      IF(Y-YL(I-1))88,96,96
   87 CONTINUE
      DX2=XF(J)-X
      SX2=0.0
      GO TO 96
   88 CONTINUE
      DX1=X-XB(J)
      SX1=0.0
      GO TO 96
   84 CONTINUE
      Z=Y+DY
      IF(Z-YU(I))96,96,85
   85 CONTINUE
      DY2=YU(I)-Y
      SY2=1.0
      GO TO 96
```

```
   96  CONTINUE
       RX=DX2/DX1
       RY=DY2/DY1
       RXY=(DX2*DX2+DX1*DX2)/(DY2*DY2+DY1*DY2)
       SFP=SF(I,J)
       SF(I,J)=((SX2+SX1*RX)+(SY2+SY1*RY)*RXY)/((1+RX)+(1+RY)*RXY)
       CH=ABS(SF(I,J)-SFP)
       IF(CH-CHM)95,95,94
   94  CHM=CH
   95  CONTINUE
   98  CONTINUE
       KZ=N4+1
       IF(I-KZ)97,97,99
   97  CONTINUE
       SF(I+N1,M+2)=SF(I,2)+1.0
        IF(I-N3)99,99,991
  991  SF(I+N1,M+2)=SF(I,2)+1.0+DELS
   99  CONTINUE
   14  CONTINUE
C
C      BLADE SURFACE VELOCITY
C
       NZ=N2+2
       NZ1=N3+1
       X=C
       WRITE(6,522)
  522  FORMAT(22H1SUCTION SIDE VELOCITY//)
       DO 51 I=NZ,NZ1
       X=X+DX
       J=1
       Y=C
   52  J=J+1
```

```
      Y=Y+DY
      IF(Y-YL(I))52,52,53
   53 A=(Y-YL(I))/DY
      UX=(1.0+A)*SF(I,J)/(A*DY)-A*SF(I,J+1)/((1.0+A)*DY)
      UY=UX*DYL(I)
      VL(I)=SQRT(UX*UX+UY*UY)
      VL(I)=VL(I)/V1
      CHORD=X/BC
      WRITE(6,59)CHORD,VL(I)
      IF(IT-1) 51,51,600
  600 IXX=I-NZ+1
      XI(IXX)=CHORD*5
      YI(IXX)=(VL(I)**2)*3.5
   51 CONTINUE
      NZ=N12+2
      NZ1=N13+1
      X=0
      WRITE(6,523)
  523 FORMAT(23H1PRESSURE SIDE VELOCITY//)
      DO 54 I=NZ,NZ1
      X=X+DX
      J=1
      Y=0
   55 J=J+1
      Y=Y+DY
      Z=Y+DY
      IF(Z-YU(I))55,56,56
   56 A=(YU(I)-Y)/DY
      VU(I)=A*(SF(I,J-1)-1.0)/((1.0+A)*DY)-(1.0+A)*(SF(I,J)-1.0)/(A*DY)
      VU(I)=VU(I)/V1
      CHORD=X/BC
      WRITE(6,59)CHORD,VL(I)
```

```
   59  FORMAT(5X,F10.5,5X,F10.5)
       IF(IT-1)54,54,601
  601  IX=I-NZ+N3-40+1
       XI(IX)=CHORD*5
       YI(IX)=(VU(I)**2)*3.5
   54  CONTINUE
C
C      STREAM FUNCTION OUTPUT
C
       WRITE(6,501)
  501  FORMAT(16H1STREAM FUNCTION//)
       NZ=N14+1
       MZ=M+2
       DO 41 I=1,NZ
       WRITE(6,42)I,(SF(I,J),J=1,MZ)
   42  FORMAT(3X,I3,14F8.5)
   41  CONTINUE
       WRITE(6,502)
   502 FORMAT(7HCCHANGE//)
       WRITE(6,503) CHM
   503 FORMAT(5X,F10.7)
   13  CONTINUE
       WRITE (6,505)
  505  FORMAT (9H1VELOCITY//)
       DO 506 I=2,N14
       JZ=M+1
       DO 507 J=2,JZ
       UX=(SF(I,J+1)-SF(I,J-1))/(2.*CY)
       UY=(SF(I-1,J)-SF(I+1,J))/(2.*CX)
       VE=SQRT(UX*UX+UY*UY)
       VEL(J)=VE/V1
  507  CONTINUE
```

```
      WRITE (6,508) I,(VEL(J),J=2,JZ)
508   FORMAT (3X,I3,12F9.4)
506   CONTINUE
      CALL PLOT(0.,0.,3)
      CALL PLOT(0.,11.0,2)
      CALL PLOT(8.5,0.0,3)
      CALL PLOT(8.5,11.0,2)
      CALL PLOT(2.0,2.3,-3)
      CALL SAXIS(0.0,0.0,INF,-16,5.0,0.0,10.0,10.0,0.5,0.5)
      CALL SAXIS(0.0,0.0,INF1 ,16,7.01,90.0,0.2101,0.2101,0.7,0.7)
      CALL SYMBOL(1.5,7.3,0.15,15HANGLE OF ATTACK,0.0,15)
      CALL SYMBOL(1.5,7.1,0.15,9H7 DEGREES,0.0,9)
      CALL SYMBOL(1.5,6.8,0.15, 23HEXIT ANGLE 2.40 DEGREES,0.0,23)
      IF(IGAM.EQ.0.) CALL SYMBOL(2.0,6.5,0.15,'1/4 SPAN',0.0,8)
      IF(IGAM.EQ.1.) CALL SYMBOL(2.0,6.5,0.15,'1/2 SPAN',0.0,8)
      IF(IGAM.EQ.2.) CALL SYMBOL(2.0,6.5,0.15,'3/4 SPAN',0.0,8)
      IF(IGAM.EQ.0.) CALL SYMBOL(3.5,6.5,0.15,'?&0=56&¬0',0.0,9)
      IF(IGAM.EQ.1.) CALL SYMBOL(3.5,6.5,0.15,'?&0=60&¬0',0.0,9)
      IF(IGAM.EQ.2.) CALL SYMBOL(3.5,6.5,0.15,'?&0=61&¬0',0.0,9)
      CALL SYMBOL(0.,-0.7,0.15,30HFIGURE   ,THEORETICAL PRESSURE,0.0,30)
      CALL SYMBOL(0.,-0.9,0.15,22HDISTRIBUTION WITH B.L.,0.0,22)
      N3C=N3-40
      DO 602 I=1,N3C
      X=XI(I)
      Y=YI(I)
      WRITE(7,604)XI(I),YI(I)
      CALL SYMBOL(X,Y,.15,1,0.,-1)
602   CONTINUE
      N3A=N3+1-40
      N3B=2*(N3-40)
      DO 603 I=N3A,N3B
      X=XI(I)
```

```
      Y=YI(I)
      WRITE(7,604)XI(I),YI(I)
      CALL SYMBOL(X,Y,.15,4,0.,-1)
603   CONTINUE
      CALL PLOT(0.,0.,-4)
604   FORMAT(5X,F10.5,5X,F10.5)
      STOP
      END
```

The vita has been removed from the scanned document

PRESSURE DISTRIBUTION ON A ROTATING AXIAL-FLOW COMPRESSOR BLADE

by

Per Erik Schultz

(ABSTRACT)

An investigation of mean rotor blade surface pressures was conducted over a range of operating conditions. The pressures were measured at three span positions and five chord positions on both suction and pressure sides.

A theoretical approach for obtaining pressure distributions on the rotor blade using simple radial equilibrium, boundary layer theory and an existing finite-difference, blade-to-blade computer program is presented.

A comparison of the experimental and theoretical pressure distribution on the rotor blade at 25 per cent, 50 per cent and 75 per cent span is included.

The comparison of experimental and theoretical pressure distribution showed, in general, good agreement.